The Centre for Australian Weather and Climate Research
A partnership between CSIRO and the Bureau of Meteorology

Australian Government
Bureau of Meteorology

CSIRO

A Spectral Climatology of Australian and South-West Pacific Tide Gauges

Stewart C. R. Allen and Diana J. M. Greenslade

CAWCR Technical Report No. 011

June 2009

www.cawcr.gov.au

A Spectral Climatology of Australian and South-West Pacific Tide Gauges

Stewart C. R. Allen[1] and Diana J. M. Greenslade[1]

CAWCR Technical Report No. 011

June 2009

[1] Centre for Australian Weather and Climate Research, a Partnership between the Bureau of Meteorology and CSIRO, Melbourne, Australia

ISSN: 1836-019X

National Library of Australia Cataloguing-in-Publication entry

Author: Allen, Stewart C. R. (Stewart Charles Richard), 1976-
Title: A spectral climatology of Australian and south-west Pacific tide gauges [electronic resource] / Stewart C.R. Allen, Diana J.M. Greenslade.
ISBN: 9781921605208 (pdf)
Series: CAWCR technical report ; 11.
Notes: Includes index; Bibliography.
Subjects: Sea level--Australia--Measurement. Sea-level--South Pacific Ocean--Measurement. Tide-gages--Australia. Tide-gages--South Pacific Ocean. Tsunami Warning System--South Pacific Ocean.
Other Authors/Contributors: Greenslade, Diana J. M. Centre for Australian Weather and Climate Research. Australia. Bureau of Meteorology. CSIRO.
Dewey Number: 551.458

Enquiries should be addressed to:
Stewart Allen
Centre for Australian Weather and Climate Research:
A partnership between the Bureau of Meteorology and CSIRO
GPO Box 1289, Melbourne
Victoria 3001, Australia
stewart.allen@bom.gov.au

Copyright and Disclaimer

Contents

List of Figures

List of Tables

ABSTRACT

This study examines the power spectrum of sea-level variability at 21 tide gauge sites around Australia and in the Southwest Pacific Ocean. It provides a first step towards understanding how sea-level variability manifests itself at individual tide gauges, and the results can be used to assess whether specific locations might be useful for tsunami detection and warning purposes.

An analysis of the inter- and intra-annual variability in the spectra shows that power spectra that are characteristic of a site can be reliably generated from time series of at least three months in length. This is based on power spectra at frequencies between 2×10^{-3} and approximately 9×10^{-2} cycles per minute (that is, periods between 12 and 1000 minutes) but holds at other frequencies beyond this range. Topographic admittance functions for all 21 sites have been calculated by assuming a specific form for the deep-water sea-level spectrum. The topographic admittance function gives an indication of the tendency for local topography at a tide gauge to amplify or attenuate observed sea-level variability within different frequency ranges.

It was found that amplification and attenuation at middle (8×10^{-3} to 4×10^{-2} cycles per minute) and high (4×10^{-2} to approximately 9×10^{-2} cycles per minute) frequencies is low at sites located within coral atolls, while amplification at these middle and high frequencies is typically large for sites located within enclosed marinas. Sites located within an open bay, but behind a large reef generally have low amplification and attenuation at all frequencies. Tide gauges in mainland locations with narrow continental shelves tend to have attenuation in the low frequency band and significant amplification in the middle and high bands. In contrast, locations with wider continental shelves tend to have a more even response through all frequency ranges, displaying milder attenuation and amplification.

1. INTRODUCTION

Observations of sea-level are essential for tsunami detection and warning purposes. This includes simple strategies such as assessing the observations subjectively to determine whether a tsunami has been generated or not, and more sophisticated uses such as incorporation into an objective data assimilation scheme. Tsunameters are excellent for this as they are located in deep water near subduction zones and can therefore provide early warning of the existence of a tsunami. However, the tsunameter network around Australia is still in development and there are few tsunameters in the region.

Tide gauges are another source of sea-level observations and the network of tide gauges is much denser. However, their ability to detect tsunamis can be problematic due to their location. Specifically, tide gauges are normally located in sheltered locations such as ports and harbours, where the mean water depth is shallow compared to the open ocean. Furthermore, any sea-level variability measured at a tide gauge that has originated from the open ocean may also have propagated onto and across a continental shelf.

When this variability is measured at a tide gauge within coastal and harbour waters, changes are observed in the spectra of total wave energy (Kulikov *et al.*, 1983). Rabinovich (1997) collated the observations of Filloux (1991) with other studies and was able to demonstrate the local transformation of the deep-water spectrum from a form that is relatively smooth and decreases in power with increasing frequency (i.e. a so-called 'red' spectrum) to a spectrum in shallow water that displays distinct spectral peaks. This is direct evidence of 'topographic admittance'. As the local bathymetry and hence admittance characteristics vary from site to site, the detection of the spectral signal for phenomena such as tsunamis and isolation of a tsunami from topographic effects is often difficult using observations from coastal tide gauges. Previous studies (eg, Rabinovich, 1997; Abe, 2001) have proposed techniques for processing coastal tide gauge records in order to isolate any tsunami spectral signal present. These techniques also allow the determination of features such as the response of the harbour to tsunamis (the topographic admittance function) and the spatially invariant spectral characteristics of a tsunami prior to entering coastal areas (the source function). Application of these methods to tide gauge data allows an understanding to be developed of how a gauge's observed spectrum might be amplified or attenuated at different frequencies by the local bathymetry and transmission over a continental shelf, where present.

Several studies have utilised these techniques, in the context of tsunami research, to understand the character of observed tsunamis at tide gauges. For example, the study of Rabinovich and Stephenson (2004) applied them in order to demonstrate that a particular tsunami event had a very different representation within a tide gauge network to observed sea-level changes linked to an intense meteorological event, i.e. a storm surge. However, these studies have all relied on two main assumptions:

- That established background spectra are truly representative of the local bathymetric response.

- That the deep-water sea-level spectrum is smooth, universal and monotonic and varies as the inverse of the square of the frequency.

This study seeks to reconsider these assumptions using longer, high-quality tide gauge records, and to develop a spectral climatology for tide gauges in the Australian region. This will allow characteristic features of these gauges to be identified with high resolution, so that they may be compared to the spectral response during unusual events including, but not limited to, tsunamis. In particular, it will allow a more thorough determination of a 'background' spectrum, necessary for calculation of quantities such as the admittance function. The use of longer time-series to produce background spectra will facilitate better spectral resolution, whilst maintaining small confidence intervals. This allows accurate determination of spectral peaks. In past studies, these background spectra have been calculated using time-series only as long as a tsunami event, typically on the order of a week. This study uses much longer time-series, up to a year in length.

This study provides a first step towards an understanding of how sea-level variability manifests itself at individual tide gauges, and the results can be used to assess whether specific locations might be useful for tsunami detection and warning purposes. This will also provide guidance for future expansion of the Australian tide gauge network.

2. THEORETICAL BACKGROUND

The theory behind this work is based largely on a simplification of the methods developed in Rabinovich (1997). We begin by considering a time series of observed sea-level at a tide gauge, $\zeta_{obs}(t)$. This time series consists of variations due to real disturbances, $\zeta_a(t)$ plus a series due to instrument noise $\varepsilon(t)$:

$$\zeta_{\text{obs}}(t) = \zeta_a(t) + \varepsilon(t) \tag{1}$$

This bears similarity with the starting point of Rabinovich (1997), except that we are including any sea-level variations due to a tsunami event within the observed time series, $\zeta_{obs}(t)$. In Rabinovich (1997), tsunami-related variations were considered separately.

Firstly, let us make comments on the treatment of the instrumental noise term. In spectral space, equation 1 transforms to

$$S_{\text{obs}}(f) = S_a(f) + S_\varepsilon(f) \tag{2}$$

where f is the angular frequency, $S_{obs}(f)$ is the spectrum of observed variability, $S_a(f)$ is the spectrum of real variability and $S_\varepsilon(f)$ is the spectrum of instrument noise. We make the assumption that $S_\varepsilon(f) << S_a(f)$, which is akin to considering only tide gauge records that have detectable background oscillations.

The effect of topography on the time-series of real variability can be quantified via a convolution of the deep-water variability, $\zeta_{dw}(t)$, and the topographic transfer function, $w(t)$:

$$\zeta_a(t) = \int_0^\infty w(\tau)\zeta_{dw}(t-\tau)d\tau \tag{3}$$

In this context, $\zeta_a(t)$ is defined as any variability that has *arrived* at the coast, i.e. has transmitted across a continental shelf (if present) and into a bay or harbour, where it has been observed by a tide gauge. Hereafter this shall be referred to as the *sea-level arrival series*. In the spectral domain, equation 3 has the form

$$S_a(f) = H^2(f)S_{dw}(f) \tag{4}$$

so that $S_a(f)$ is the *sea-level arrival spectrum,* $S_{dw}(f)$ is the *deep-water spectrum* and $H(f)$ is a function describing the transformation of the deep-water spectrum by the coastal topography.

Therefore, given an observed spectrum and an assumed form of S_{dw} we may determine the admittance function

$$H(f) = \sqrt{S_a(f)/S_{dw}(f)} \tag{5}$$

This provides a basis for quantifying the tendency for local topography at a tide gauge to amplify or attenuate observed sea-level variability. Values of $H(f)$ greater than one indicate amplification by the topography, values less than one indicate attenuation, while values equal to one indicate unaltered transmission of the deep-water power at that frequency and no modification by local topography. The choice of an appropriate form for $S_{dw}(f)$ will be discussed in section 5.

Rabinovich (1997) importantly points out that $H(f)$ is not a simple, invariant function of frequency alone. For example, in the case of a tsunami event, it will vary with the angle of incidence of waves arriving at the coast. This also implies that it might vary if it is derived from data at different time scales. We aim to examine this aspect of the function by using time series of observations of different length that would encompass waves incident from all possible angles of incidence.

3. DATA AND METHODOLOGY

This work requires a reasonably long data stream of good quality tidal records from a number of tide gauges. The Bureau of Meteorology, through the National Tidal Centre (NTC), is responsible for maintaining and archiving data from a large number of Australian and regional tide gauges. The tide gauges that will be included in this study are SEAFRAME (Sea-level Fine Resolution Acoustic Measuring Equipment) stations used in two networks: the Baseline Array, which covers tide gauges in Australian waters installed as part of the Australian Baseline Sea-Level Monitoring Project, and the Pacific array, which covers gauges in the South Pacific and forms part of the South Pacific Sea-Level and Climate Monitoring Project.

The standard SEAFRAME tide gauge samples observations of sea-level every second and records both 1-minute averages (every minute) and 3-minute averages (every 6 minutes). Historically, the 1-minute observations were only downloaded from the gauge and archived by NTC in the event of a tsunami. With the advent of the Australian Tsunami Warning System (ATWS) communication upgrades have allowed the 1-minute data to be routinely transmitted in real time and archived since approximately December 2006. These data have a relatively high Nyquist frequency of 0.5 cycles-per-minute (cpm), which is suitable for use in the examination of features such as tsunamis. However, they are often plagued by gaps arising from instrument errors and communication failures.

The 6-minute sea-level data are the primary quality-controlled dataset, which, despite having a relatively low Nyquist frequency of approximately 0.08 cpm, have far fewer gaps than the 1-minute records and are considerably more complete. Furthermore, in contrast to the archive of 1-minute observations, the 6-minute observations have been routinely archived for all SEAFRAME sites since their installation, mostly in the early 1990's. The length of their record makes them an ideal data source for this study.

Records of 6-minute observations for 21 'key' Baseline and Pacific tide gauges were examined for completeness and continuity. Key sites are defined as those where a tsunami event has previously been observed in the tide gauge record. Their locations are shown in figure 1 and details are given in table 1, along with the date of installation of each gauge. It was found that for these key sites, the 6-minute data were at least 98.9% complete for the years 2001, 2002 and 2006, with the majority of sites being 100% complete for these years. Data series that were not complete were filled using least-squares quadratic splines. The variability of the spectral response over different years will be investigated using these data.

Furthermore, data for 2002 were uninterrupted over 12 months for all sites shown in figure 1 and table 1, bar four (The Marshall Islands, Nauru, Samoa and Tonga). On this basis, data for this year were used to investigate the variability on intra-annual time-scales at the key sites.

The analysis of the observations here is performed on the raw tide gauge data, i.e. tidal predictions have not been removed from the observations. This means that tidal peaks are very evident in the spectra and also in the topographic admittance functions. This could be avoided by removing the known tidal signal before performing the analysis; however, techniques used for removing the tidal signal were not deemed to be satisfactory for this study. Simply subtracting the predicted tide from the observations often does not remove all the tidal variability, and removing the tidal signal using filtering methods is likely to remove some of the variability that we are interested in here. For this reason, the analysis was performed using raw observations, without removal of the tidal signal.

Power spectra of time series were calculated using Fast Fourier Transforms (FFT). The FFTs were ensemble averaged using a Kaiser-Bessel window with half-window overlaps. The window was chosen to be 2048 time-steps in length (i.e. 12288 minutes), which yields 166 degrees of freedom. 95% confidence intervals are determined for each spectrum.

4. INTER- AND INTRA-ANNUAL VARIABILITY OF TIDE GAUGE SPECTRA

In order to examine the variability of tide-gauge spectra across different years, power spectra for the years 2001, 2002 and 2006 were calculated for all sites shown in figure 1. Spectra are shown for the Cocos Islands and Spring Bay, as examples, in figures 2 and 3, respectively. These sites are chosen here as they display very different spectral responses. The spectra in each figure exhibit several features of note. The most prominent aspect is that there is very little difference in the spectra between years (highlighted by the fact that the three spectra are nearly indistinguishable from one another in figures 2 and 3). Any variability between years is well within the 95% confidence interval marked on the plots. Spectra for other sites not shown also show very little variability amongst the years.

In the spectra for both sites, there are a number of strong, distinct peaks at the lower end of the frequency range. In particular, all have their strongest peak centred at approximately 0.0013 cpm (that is, approximately 12 hours), corresponding to the semi-diurnal tidal constituents. Not shown on the spectral plots is a peak of similar power centred at approximately 24 hours that corresponds to diurnal tidal fluctuations. There are a number of other peaks that are common to the spectra of these sites and all other sites. These also occur in the lower frequency bands of the spectra, with periods around 485, 370, 295 and 245 minutes and correspond to non-linear, shallow-water overtidal constituents (Parker, 1991).

It should be noted that these spectra demonstrate one of the advantages of calculating spectra from long time series: the spectra can be generated with longer windows. This allows for excellent frequency resolution, but still maintains a high number of degrees of freedom and small confidence intervals. This is in contrast to studies that have generated spectra from time-series only as long as, say, a tsunami event and hence are not able to resolve these peaks while maintaining a small confidence interval.

Given that interannual variability of the present sea-level spectra is small (for the frequencies considered), spectral variability on sub-annual time scales is now investigated. Spectra of observations for 2002 were calculated at all sites for shorter periods, specifically six months, three months and one month. The spectra were ensemble averaged with a 2048 time-step (i.e. 12288 minute) Kaiser-Bessel window. These windows yield 166, 82, 38 and 10 degrees of freedom, as the length of the series decreased from twelve months down to one month.

The ensembles of these spectra, for Cocos Islands and Spring Bay (again, as examples), are shown in figures 4 and 5 respectively. The yearly spectra are also shown for comparison. In each of the figures (except, of course, the yearly spectra), the black line shows the mean of the set of spectra and the grey shading encompasses the spread of the set. 95% confidence intervals are indicated on the spectra.

The mean spectra produced from the shorter series in these figures are very similar to the yearly spectrum, with the locations of the peaks in frequency space showing very close correspondence between the different spectra. Also, the spread of the set of spectra shows there is little variability in spectra, provided they are generated from three-month time-series or longer. However, for monthly time-series, the variability increases markedly. This is likely to be due not only to real variability, but also to a decrease in the number of degrees of freedom and associated increase in the span of the 95% confidence interval.

Whilst these results have only been shown for two sites, they are consistent across the 21 sites considered in this study and suggest that power spectra characteristic of a site can be reliably generated from time series of at least three months in length for frequencies between 2×10^{-3} and approximately 9×10^{-2} cycles per minute (that is, periods between 12 and 1000 minutes).

5. SOME CONSIDERATIONS OF THE DEEP, OPEN OCEAN SPECTRUM

As seen in equation (5), accurate estimates of the topographic admittance function *H(f)* are dependent on knowledge of the form of the deep water spectrum, $S_{dw}(f)$. Previous studies analysing bottom pressure measurements of sea-level (e.g. Kulikov *et al.*, 1983 and Filloux *et al.*, 1991) have found that the high-frequency band (2×10^{-3} to 5×10^{-1} cpm) of the deep-water spectrum is smooth, monotonic and almost universal. It can be expressed as

$$S_{dw}(f) = A_0 f^{-2} \tag{6}$$

where the value of the constant A_0 in equation 6 has been estimated to be in the range of 10^{-3} to 10^{-4} $cm^2 \cdot cpm$ in large open ocean basins and an order of magnitude higher in smaller seas due to energy conservation (Filloux, 1991).

The current rapid expansion of the global tsunameter network will provide an opportunity to examine these findings in greater detail. In particular, it will enable the exploration of the dependence of the form of Equation 6 on parameters such as water depth, geographic location, etc. In the Australian region, at the time of writing, there is only one tsunameter with a long enough time series of suitable observations to permit analysis. This is the tsunameter located near the Puysegur subduction zone (see figure 1).

Uninterrupted data from this sensor, with a sampling interval of 15 minutes, were obtained for approximately 94 days. The power spectrum was calculated in the manner described in section 3, but with a window of 1024 time steps (i.e. 15360 minutes) and 30 degrees of freedom. The resulting spectrum is shown in figure 6. Note that as in the tide gauge spectra, the semi-diurnal peak is evident here. In addition, several overtidal constituents also appear, suggesting that these are not in fact specific to shallow water.

This spectrum displays a form similar to that of equation 6 for frequencies between approximately 2×10^{-3} cpm and the series' Nyquist frequency (around 3.3×10^{-2} cpm). This was confirmed using a least-squares regression, which suggested an exponent between -2.2 and -1.8, depending on the lower bound of the chosen frequency range. Thus we can be confident regarding the assumption of an f^{-2} slope in the deep-water spectrum.

We examine now the value for A_o. The two dashed lines on figure 6 represent two different values of A_o; the upper line is $A_o = 10^{-4}$, and the lower line is $A_o = 10^{-6}$. It is clear from this figure that the value of 10^{-6} is more appropriate for this particular spectrum. This is somewhat different to that found by other authors. It is not clear why this is so, and it deserves further investigation. Possible reasons for the differences are geographical and temporal variability and differences in tsunameter measurement techniques.

For the current work, we will use the value $A_o = 10^{-4}$, as this has been used most often by previous authors, allowing comparison with past studies. It should be borne in mind, however, that given the potential uncertainty relating to the value of A_o, the most useful information to be gained from the remainder of this report is in the comparison of the admittance functions of each site relative to one another, rather than considering their absolute values.

6. TOPOGRAPHIC RESPONSE AT AUSTRALIAN TIDE GAUGES

In this section, the spectrum and related topographic response at each of the key sites in figure 1 are analysed and discussed. The sites are discussed in two groups, the Australian Baseline Array gauges and the Pacific Array Gauges. Given the results of section 1, the spectra are calculated with 2002 data. This approach allows a high degree of confidence that the spectra will be characteristic of each site.

Recall that all sites except four, have no missing data in this year. The sites with missing data - Marshall Islands, Nauru, Tonga and Western Samoa - have at least 8 consecutive months of continuous data. Although section 1 showed that as little as three months of data can be used to produce spectra that are characteristic of the site, it makes sense to use all data that is available. In a similar vein, rather than attempting to fill gaps with splines, the longest possible complete time series was taken (to the nearest whole month) for these four sites in order to increase confidence in the results.

6.1 Australian Baseline Array Gauges

6.1.1 Broome, Western Australia

The Broome tide gauge is situated at the end of a jetty on the leeward side of a peninsula and is near the mouth of Roebuck Bay, which is approximately 20 km in diameter. The continental shelf in this region is relatively wide, extending approximately 500 km from the coastline. The tidal range at Broome is very large and may be as much as 10 m between successive high and low tides during the spring phase.

The power spectrum for Broome is shown in figure 7a. Also shown on this figure is a curve parallel to the hypothetical deep-water spectrum (equation 6). Figure 7b shows the resulting admittance function for Broome, as calculated from these spectra.

There are a large number of distinct spectral peaks in the low and middle frequency ranges. As in section 1, the largest peak can be linked to a semi-diurnal tidal period. Other overtidal peaks occur at periods of approximately 6, 4, 3 and 2.5 hours. As will be shown, the Broome sea-level spectrum displays many more peaks in the low frequency range than any other site. However, in higher frequency regions, the signal tends to be attenuated. This is readily seen in figure 7b, where the admittance function has values less than unity for virtually all frequencies higher than approximately 0.007 cpm (i.e. periods shorter than approximately 140 minutes).

6.1.2 Cape Ferguson, Queensland

The Cape Ferguson tide gauge is located on a jetty that extends from the headland of a large bay approximately 40 km across by 15 km wide. This bay is open to the northeast and is separated from the Coral Sea by the Great Barrier Reef approximately 50 km away and by the continental shelf, which extends out to approximately 100 km.

Figure 8a shows the power spectrum for Cape Ferguson and figure 8b, the corresponding admittance function. As observed at other sites, there is a dominant semi-diurnal tidal peak and several other overtidal peaks, although the peaks are generally smaller compared to Broome.

At higher frequencies, there are some variations in power, but overall, the admittance function remains close to one. This implies there is little amplification or attenuation of incoming wave energy at Cape Ferguson over the frequencies considered.

6.1.3 The Cocos (Keeling) Islands, Western Australia

The Cocos Islands tide gauge is located at the end of a concrete pier, which extends from a coral atoll into a lagoon. This lagoon has a length scale the order of 10 km and is surrounded by deep ocean.

Figure 9a shows the power spectrum for Cocos Islands and figure 9b, the corresponding admittance function. From the spectrum, apparent tidal fluctuations are weaker here than at other sites. The semi-diurnal tidal peak is strong, as at other sites, but other observed tidal peaks are notably smaller. The entire spectrum is mostly parallel to the assumed deep-water spectrum, with no strong distinct peaks, although there is a slight whitening of the spectrum at higher frequencies. This implies that the deep-water signal may arrive at the Cocos Islands tide gauge without significant alteration by local topography. This is evident in figure 9b, where the admittance function is close to unity for most frequencies up to 0.05 cpm.

6.1.4 Esperance, Western Australia

The Esperance tide gauge is located within a deep port that is sheltered from the open ocean by a headland. The continental shelf is approximately 80 km wide in this region.

Figure 10a shows the power spectrum for Esperance and figure 10b, the corresponding admittance function. The spectrum for this site is strikingly different to those discussed above. Firstly, the power in the semi-diurnal tidal peak is notably smaller than other sites discussed so far. Note that it is well known that semi-diurnal tides are relatively small along southern Australia (Chittleborough, *pers. comm.*). Furthermore, the overall spectral response across all frequencies is relatively even and does not display the drop-off in power with increasing frequency. The spectrum displays several broad low-power peaks.

Consequently, the admittance function shows amplification by the topography from approximately 0.005 cpm, which increases significantly with frequency. This is a direct result of the whitening of the assumed 'red' deep-water spectrum. The broad peaks mentioned above are more visible in the admittance function and suggest amplification between 5 and 10 times at some frequencies.

6.1.5 Hillarys, Western Australia

The tide gauge at Hillarys is situated within a boat harbour and marina at a very sheltered location. The opening of this marina is relatively narrow and there are many piers for boat mooring within. The continental shelf in this location extends approximately 80 km from the coast.

Figure 11a shows the power spectrum for Hillarys and figure 11b, the corresponding admittance function. This spectrum shares some features with the spectrum calculated for Esperance. The semi-diurnal peak is one of the weakest of all sites. The other tidal peaks in the low frequency end are also relatively weak. However, overall the spectrum also has a reasonably even response across all frequencies.

The admittance function reveals differences between the Hillarys and Esperance spectra. The white nature of the spectrum produces an admittance function that tends to increase significantly with increasing frequency. However, unlike Esperance, there is a band near 0.010 to 0.015 cpm that has relatively low amplification and the highest values of the admittance function are limited to the highest frequencies.

6.1.6 Port Kembla, New South Wales

Port Kembla is a large, industrial seaport with a harbour protected by sea walls. The tide gauge is located near the shore end of a jetty that makes up part of a marina. Hence it is located in a relatively sheltered location. The continental shelf is relatively narrow, compared to other mainland sites, extending out approximately 50 km.

Figure 12a shows the power spectrum for the Port Kembla tide gauge and the corresponding admittance function is shown in figure 12b. The semi-diurnal peak shows relatively high power, especially compared to Hillarys, a site also located within an enclosed harbour, and Esperance, another large port. Other low-frequency peaks are small, but are embedded within a spectrum that decreases with increasing frequency, proportional to the assumed deep-water spectrum. However, at frequencies higher than approximately 0.01 cpm, there is significantly more power in the spectrum, with several peaks.

The admittance function reflects this, with frequencies between the semi-diurnal peak and approximately 0.01 cpm showing considerable attenuation, but frequencies higher than this showing amplification. The amplification is often less than a factor of 5, except for three peaks: a narrow peak near 0.015 cpm with an amplification factor around 5, and two broad peaks near 0.04 and 0.07–0.09 cpm with amplification factors around 10.

6.1.7 Portland, Victoria

The tide gauge at Portland is on a jetty within Portland Bay. The jetty is sheltered from the open ocean by a headland and breakwater. The continental shelf is narrow, extending approximately 40 km offshore.

The spectrum for Portland is shown in figure 13a and the admittance function in figure 13b. The semi-diurnal tidal peak in the spectrum is a similar size to that observed at other sites, however the overtidal peaks are relatively small. The spectrum is slightly ‘red’ towards higher frequencies, but contains some broad regions of higher power in the mid frequency range.

The admittance function in figure 13b suggests some fairly large amplification across mid and high frequencies between 2 and 5 times, with a maximum near 0.03 cpm.

6.1.8 Rosslyn Bay, Queensland

Rosslyn Bay is a sheltered marina near Yeppoon. The tide gauge is located on a pier within this marina in a relatively sheltered location. This site is just to the south of the Great Barrier Reef, and the continental shelf is approximately 300 km wide at this location.

Figure 14a shows the power spectrum for the Rosslyn Bay tide gauge sea-level signal and the corresponding admittance function is shown in figure 14b. The low-frequency peaks for Rosslyn Bay resemble those at nearby Cape Ferguson. There is also a general ‘red’ decrease in spectral power with increasing frequency, however, it is not as marked as at Cape Ferguson. This results in some apparent amplification in the admittance function. At moderate frequencies (that is, from 0.006 to 0.03 cpm), this amplification is about a factor of 2. At higher frequencies, this increases to a factor of approximately 4.

6.1.9 Spring Bay, Tasmania

The tide gauge at Spring Bay is located at the end of a short pier, which is sheltered from open water by a larger pier. Spring Bay opens into Mercury Passage, with Maria Island just beyond the bay entrance.

Figure 15a shows the power spectrum for Spring Bay and figure 15b, the corresponding admittance function. This spectrum displays many of the features observed at other sites: a strong semi-diurnal tidal peak, other distinct but smaller peaks in the low-frequency range, a general redness of the overall spectrum but with some increase at the upper end. However, this spectrum shows an unusual band of high spectral power between 0.01 and 0.03 cpm.

This band of high spectral power produces an unusual admittance function as shown in figure 15b. There is a region of (mostly) attenuation, between the semi-diurnal peak and approximately 0.01 cpm and mild amplification at the upper frequency end. However, the strongest amplification occurs between 0.01 and 0.03 cpm. Here, amplification by a factor of approximately 3, but there are peaks indicating topographic amplification by a factor approximately between 5 and 12.

6.1.10 Thevenard, South Australia

The Thevenard tide gauge is sited on the coastal side of a long jetty in Murat Bay at the north-western shores of the Eyre Peninsula. The bay has a length scale of approximately 5 km and is sheltered from the open water by St Peter Island. The continental shelf in this area is approximately 250 km wide.

The spectrum for Thevenard is shown in figure 16a and the admittance function in figure 16b. The semi-diurnal tidal peak is relatively strong, as are other nearby low-frequency peaks. Low-frequency power is also generally high, which results in some amplification in the admittance function between 0.003 and 0.01 cpm by a factor of approximately 2 to 4 times. However, at higher frequencies, there is little amplification, with the admittance function remaining approximately at unity.

6.2 Pacific Array Gauges

6.2.1 Rarotonga, the Cook Islands

This tide gauge is located on the northern coast of the island of Rarotonga within Avarua harbour. The harbour is small and triangular in shape with a length scale of approximately 300 m. The island is surrounded by lagoon waters that extend a few hundred metres to a reef. Beyond the reef are deep open-ocean waters.

The spectrum for Rarotonga is shown in figure 17a and the admittance function in 17b. Compared to other sites, the spectrum is relatively ‘flat’ and has relatively small tidal peaks (with the exception of the semi-diurnal peak). It has a decrease in power with increasing frequency, except in the high-frequency range where there is an increase in power.

These features are clearly represented in the admittance function. The function is less than unity at all frequencies up to approximately 0.04 cpm. At high frequencies, the admittance function suggests increasing amplification with frequency up to 3 times in magnitude.

6.2.2 Lautoka, Fiji

The Lautoka tide gauge is located on the northwest coast of the island of Viti Levu in Fiji. The gauge is within a port that is located in a channel that is approximately 250m wide and 750m long and bound by Viti Levu and another smaller island. The area is in proximity to a number of coastal reefs and islets and the open ocean is approximately 50km away.

Figure 18a shows the spectrum for the Lautoka tide gauge. The semi-diurnal tidal peak shows relatively high power, but the overtidal peaks, though clearly distinguishable, are significantly weaker. As the spectrum drops off with increasing frequency, there are a number of broad sections of slightly increased power. The largest occurs between 0.004 cpm to 0.008 cpm.

The Lautoka admittance function, shown in figure 18b, shows that at low frequencies (less than 0.005 cpm) there is mostly attenuation, while at higher frequencies, the admittance function is mostly unity, or slightly above unity, indicating small amplification of the signal by topography. This amplification, however, is never greater than 2 times.

6.2.3 Kiribati

The Pacific Array tide gauge at Kiribati is located at Betio Port, which is located within the sheltered lagoon of Tarawa Atoll. The lagoon has a length scale of approximately 25 km and is open to the ocean to the west.

The spectrum for Kiribati is shown in figure 19a and the admittance function is shown in figure 19b. The spectrum is slightly unusual compared to spectra examined at most other sites. Although the semi-diurnal tidal peak is large, the higher-frequency overtidal peaks are much smaller. At low frequencies, the spectrum has quite constant power up to 0.007 cpm, at which point it drops significantly. There are some minor peaks at higher frequencies, but the spectrum in this section is more typically ‘red’.

The admittance function shows amplification up to 3 times in magnitude for low frequencies up to 0.07 cpm. At higher frequencies, the function shows slight attenuation, except near 0.015 and 0.03 cpm, where the function is near unity.

6.2.4 Marshall Islands

The Marshall Islands tide gauge is located on Majuro Atoll. The atoll encloses a lagoon that has dimensions approximately 40 km by 10 km. The tide gauge is located within this atoll on the eastern edge. The lagoon atoll opens to the deep ocean at its northern edge.

Figure 20a shows the spectrum for the Marshall Islands tide gauge. Due to missing data between mid September and mid October, this spectrum has been calculated using 8 months of data from 1 January to 1 September, 2002.

In the lower frequency section of the spectrum, the overtidal peaks are distinguishable but not as strong as at many other sites. The spectrum shows only a weak ‘red’ decrease in power with increasing frequency in the lower end of the spectrum with no unusual peaks. From approximately 0.01 cpm, the spectral power drops considerably towards the high-end of the spectrum. There are distinct peaks near 0.02, 0.035, 0.045, 0.065 and 0.075 cpm.

The admittance function in figure 20b shows mild amplification by a factor of approximately 2 up to about 0.01 cpm. Above this, there is generally mild attenuation. However, the high-frequency peaks identified in the spectrum produce amplification, with the peak near 0.035 cpm suggesting amplification by a factor of approximately 4.

6.2.5 Nauru

The tide gauge at Nauru is located on the western shore of the island within a small, enclosed, man-made harbour. The island is surrounded by deep water.

The spectrum for Nauru is shown in figure 21a. There was missing data at this site between January and mid April. Therefore the spectrum is calculated using a shorter time series spanning 1 May to 31 December, 2002.

The Nauru spectrum is quite unusual when compared to spectra at other sites. There are no overtidal peaks visible, nor any other notable peaks at higher frequencies. There is a 'red' decrease with increasing frequency that flattens off at approximately 0.03 cpm.

The admittance function, shown in figure 21b, suggests moderate amplification across all frequencies, before increasing markedly from 0.03 cpm, the point where the spectrum ceases to decrease. The admittance function for Nauru could be described as being similar in form to that of the Cocos Islands, except there is, overall, a greater amount of amplification, particularly at high frequencies.

6.2.6 Manus Island, Papua New Guinea

The tide gauge on Manus Island is located on the eastern end of the island's northern shore at the township of Lombrum. It is on a jetty that is located within a small bay with a length scale of approximately 1.5 km. This bay is located within a much larger inlet that is sheltered from the open ocean to the north by an archipelago of islands. There is a continental shelf that is approximately 150 km wide.

The spectrum for Manus Island is shown in figure 22a. Compared to other sites, the semi-diurnal peak is relatively weak. It shows spectral power of approximately 10^3 cm^2/cpm and, along with Hillarys and the Solomon Islands, is one of the weakest semi-diurnal peaks. Overtidal peaks are distinguishable at approximately 8, 6 and 5 hours. The spectrum has a typical 'red' decrease with some broad peaks of increased power in the mid and high frequencies.

These peaks produce quite an interesting admittance function, shown in figure 22b. The function is close to unity at low frequencies up to approximately 0.01 cpm, where there is a large band of amplification up to 5 times in magnitude for frequencies between 0.01 and 0.02 cpm. At higher frequencies, there are other smaller peaks of amplification (up to 2 times in magnitude) in between regions of weak attenuation.

6.2.7 Samoa

The tide gauge at Samoa is located at the port of Apia on the northern shores of the island of Upolu. It is located in a fairly sheltered location within the harbour, whose entrance is flanked by reefs and sand bars.

The Samoa tide gauge spectrum is shown in figure 23a. This site had a period of missing data during 2002 from early October to mid December. Therefore, the spectrum was calculated using a time series spanning 1 January to 1 October, 2002.

The spectrum shows a semi-diurnal tidal peak that is strong, but not unusually so. Overtidal peaks are present, but are weak and relatively broad compared to other sites. The usual decrease in power with increasing frequency is present but becomes flatter from approximately 0.016 cpm and increases slightly at the highest frequencies. There is a broad peak at approximately 0.04 cpm.

The admittance function is seen in figure 23b. It is near unity around most of the overtidal peaks and shows moderate attenuation elsewhere. From 0.03 cpm, the function increases to suggest amplification. The peak identified in the spectrum near 0.04 cpm suggests amplification by a factor of 2-3, and at higher frequencies, the function shows increasing amplification up to a factor of 4.

6.2.8 Solomon Islands

The Solomon Islands tide gauge is located at the end of a jetty in Honiara on the northern shores of the island of Guadalcanal. It faces into the Solomons archipelago and so is sheltered from the open ocean.

The spectrum for this site is shown in figure 24a. There are a number of relatively large overtidal peaks. These peaks decrease in power with increasing frequency, but those at the lower end of the spectrum are comparable in magnitude to the relatively small semi-diurnal tidal peak. These tidal peaks may be reflective of the relatively sheltered location of this gauge. Apart from these peaks, there are no other features of note in this spectrum. There is the usual 'red' decrease in power, with a sharp drop near 0.02 cpm.

The admittance function, presented in figure 24b, shows weak attenuation across all frequencies with the tidal peaks superimposed. The drop in spectral power near 0.02 cpm results in an increase in the level of attenuation over high frequencies.

6.2.9 Tonga

The tide gauge at Tonga is located at the Nuku'alofa container terminal in a small enclosed harbour on the northern shores of the island. It is separated from the deep, open ocean by a region of shallow water approximately 20 km in scale.

During 2002, there was some missing data for the Tonga tide gauge during December. Therefore the spectrum was calculated using a time series spanning 1 January to 1 December, 2002.

The spectrum, shown figure 25a, shows a number of overtidal peaks that accompany the semi-diurnal tidal peak. Otherwise, the spectrum shows a decrease in power with increasing frequency. The only features of note are a broad peak in power between 0.01 and 0.02 cpm and an increasing shift in power at 0.03 cpm.

These features are evident in the admittance function, shown in figure 25b. There is mostly moderate attenuation in the low and mid frequencies, but a broad peak between 0.01 and 0.02 cpm produces amplification by a factor of between 2 and 3. The shift in power identified in the spectrum at 0.03 cpm tends to shift the admittance function from mild attenuation at low frequencies to near unity for frequencies higher than 0.03 cpm.

6.2.10 Tuvalu

The Tuvalu tide gauge is located on a jetty on the islet of Fongafale. The Tuvalu atoll encloses a lagoon roughly 15 km in diameter, in which the tide gauge is located. Therefore, the gauge is relatively sheltered from the deep ocean.

Figure 26a shows the spectrum for the Tuvalu tide gauge. It is clear that although the main tidal peak is high in power, the overtidal peaks at this site are relatively small. The spectrum decreases in power with increasing frequency up to 0.03 cpm. At higher frequencies, the spectral power is reasonably constant. This spectrum bears close resemblance to spectra observed at the Cocos Islands, the Cook Islands and Nauru.

The admittance function for Tuvalu is shown in figure 26b. As might be expected from the discussion of the spectrum above, there is weak attenuation across most frequencies. The exception is the upper end of the domain, where from 0.05 cpm, the admittance function shows weak amplification.

6.2.11 Vanuatu

The Vanuatu tide gauge is located at Port Vila on the island of Efate. It is in a relatively sheltered location behind a headland in a small basin. This basin is connected to a larger bay that is open to the ocean. The excitation of oscillations within this bay by tsunamis has been considered by others (e.g. Chittleborough, unpublished document).

Figure 27a shows the spectrum for the Vanuatu gauge. Many of the usual features can be observed; there is a clear semi-diurnal tidal peak and several other overtidal peaks. There are few other features of note, except for a large region of increased power between approximately 0.03 and 0.07 cpm.

The admittance function for Vanuatu is shown in figure 27b. It shows fairly strong attenuation at all frequencies, except between the band identified above in the spectrum between approximately 0.03 and 0.07 cpm. In this band there is strong amplification by a factor of 3 to 6. In particular, the highest peak of power occurs close to 0.04cpm (specifically with a period of 24 minutes). This is very close to the period of a dominant peak of power found by Chittleborough (unpublished document), who further demonstrated that it arises from seiching within the largest bay in which the gauge is located.

7. DISCUSSION

The 21 sites examined here have resulted in quite different topographic admittance functions, with some sites amplifying low frequency variability, some amplifying high frequencies and others with a mixed response. Table 2 shows a classification of the response of the tide gauges for different frequency 'bands'. In this case, low frequency is considered the range 2×10^{-3} to 8×10^{-3} cpm (periods between 8.3 hours – 2.1 hours), middle frequency is considered the range 8×10^{-3} to 4×10^{-2} cpm (2.1 hours – 25 minutes) and high frequency is considered the range 4×10^{-2} to approximately 9×10^{-2} cpm (25 minutes – 12 minutes). The degree of attenuation or amplification is given a grade between -3 and +3 respectively with larger magnitudes indicating more. Negative values imply attenuation while positive imply amplification. In instances when there is both a negative and positive number, it indicates there is mostly attenuation, but with one or more significant peaks of amplification, or vice-versa.

Within table 2, the sites are also categorised broadly into their type of site. That is, whether it is within a bay, marina or atoll and whether it is sheltered or open to the deep ocean. For sites located on the mainland, an approximate width of the continental shelf is also listed.

It is difficult to draw any firm conclusions, however there are some interesting points of note. With respect to site type:

- Amplification and attenuation is generally low at sites located within coral atolls and at sites within an open bay but behind a large reef.
- Contrastingly, amplification at middle and high frequencies is typically large for sites located within enclosed marinas.
- Sites in the other type categories show a wide range of responses and hence conclusions are hard to draw.

If the response at mainland sites is considered with respect to the local width of the continental shelf, it appears that those sites located near narrow shelves (say, less than 100km) tend to have attenuation in the low-frequency band and significant amplification in the middle and high bands. In contrast, those with wider continental shelves tend to have a more even response in each frequency band, displaying milder attenuation and amplification.

A number of sites display spectra that do not appear to have any distinct non-tidal spectral peaks, particularly at higher frequencies. This suggests that local topography does not significantly alter incoming signals from the open ocean. Observations from these sites, namely Cocos Islands, Cape Ferguson and Tuvalu, might be useful in determining the deep-water character of tsunamis and other oceanic events. However, the paucity of deep-water observations has only allowed us to make a relative determination at this stage, that is, these sites do not amplify incoming signals, relative to other sites. Once suitable deep-water observations become available, more rigorous determinations of the deep-water spectra could enable this list to be verified in absolute terms and possibly extended to include the gauges at Nauru and Cook Islands. In some instances, further analysis might indicate that tsunami observations from 'strategically' located sites (such as Cocos Islands) are potentially suitable for assimilation into numerical models of deep-water tsunami propagation. Sites where the topographic admittance function differs markedly from a value of one across typical tsunami periods are suitable for the purpose of verifying the existence of tsunamis and also for the verification of tsunami models capable of resolving coastal bathymetry and non-linear shallow-water dynamics.

If the expected response of sites to incoming wave energy is known, it may be possible to account for local response in the event of an approaching tsunami. At the very least, it may be possible to qualitatively understand the local response, even if quantitative predictions cannot be made. For example, there were many observations of the tsunami caused by the Great Sumatra-Andaman earthquake of 26 December 2004. The maximum tsunami wave height observed at the nearby Cocos Islands was on the order of 60 cm (Allen and Greenslade, 2007; Rabinovich and Thompson, 2007). This was significantly smaller than the wave heights observed at Hillarys (~120 cm) and Esperance (~90 cm), despite those sites being much further from the tsunami source. These observations can be linked to the spectra and admittance functions shown in section 6 for these sites. Previous studies (Allen and Greenslade, 2007; Rabinovich and Thompson, 2007) have shown that most spectral power associated with the tsunami occurred at frequencies higher than 0.01 cpm (i.e. periods shorter than 100 min). At frequencies higher than this, the gauge at the Cocos Islands showed mostly either attenuation or no modification, while the Hillarys and Esperance gauges showed strong amplification. This information might be useful for forecasters in issuing warnings and may give an indication where impacts might be greater than expected if local effects are not considered. However, since it only provides information for a specific site, it should be used in conjunction with other tools such as numerical modelling of the tsunami propagation and dynamics.

8. SUMMARY AND FURTHER WORK

This study has examined the power spectrum of sea-level variability at a number of tide gauge sites around Australia and in the southwest Pacific Ocean. Power spectra have been calculated using as much as 1 year of data in order to produce fine spectral resolution at tidal and higher frequencies. This has allowed for the capture of characteristics of spectral variability observed at each site. By making assumptions about the power spectrum in the deep, open ocean, we have attempted to quantify the effects of local topography at each site.

As discussed in section 5, recent deep-water observations suggest the assumed theoretical form of the deep-water spectrum (see equation 6) should be re-examined. With a rapidly increasing network of deep water observing stations, both in the Australian region and globally, the profile assumed in this study could be further verified, and the variability of the form of the spectrum in different ocean basins could be established.

The only source of uninterrupted tide gauge data currently available over a long time period has a 6-minute temporal resolution. Compared to other data sources (e.g., 1-minute observations), these observations are relatively coarse. The limitation in using them is that they have a lower Nyquist frequency and may not be able to resolve some frequencies generated by tsunamis. However, as noted in section 3, recent changes in procedures have resulted in full archival of one-minute tide gauge observations, rather than just during tsunami events. As the archive of one-minute observations grows, these calculations could be repeated using this higher-frequency data set.

Recently, authors have been employing wavelet analysis and other time-frequency techniques to examine tsunamis within tide gauge records (e.g. Rabinovich and Thompson, 2007; Pattiaratchi and Wijeratne, 2008). It is argued that this technique is more appropriate than conventional spectral analysis, as on short time scales (i.e. hours to days), tsunamis appear as strongly non-stationary processes. However, there are currently no known techniques for estimating or removing topographic effects when using wavelet analysis. Therefore, it would be useful to investigate whether a method similar to that employed in this study could be developed to investigate topographic influence on tide gauge records, but within a wavelet analysis context.

ACKNOWLEDGEMENTS

The authors would like to acknowledge Paul Davill and Daryl Metters for providing the NTC data, Jane Warne for useful discussions and Paul Sandery, James Chittleborough and Gary Brassington for reviewing the document.

REFERENCES

Abe, K., 2001. Exclusion of a coastal effect from tsunamis recorded at ports in the use of the observed seiche. In: Intern. Tsunami. Symp. 2001, Seattle, WA, 7 August 2001, pp. 611-618

Allen, S. C. R. and D. J. M. Greenslade, 2007. The potential use of coastal tide gauge data in the Australian tsunami warning system. *IUGG XXIV General assembly*, Perugia, Italy.

Chittleborough, J., unpublished document. Excitation of harbour oscillations at Port Vila, Vanuatu by tsunamis.

Filloux, J. H., D. S. Luther and A. D. Chave, 1991. Update on seafloor pressure and electric field observations from the north-central and northeastern Pacific: Tides, infratidal fluctuations and barotropic flow. In *Tidal Hydrodynamics*, B. B. Parker (Ed.), pp 617-639, John Wiley, New York

Kulikov, E. A., A. B. Rabinovich, A. I. Spirin, S. L. Poole and S. L. Soloviev, 1983. Measurement of tsunamis in the open ocean. *Marine Geodesy*, **6**, 311-329.

Parker, B. P., 1991. The relative importance of the various nonlinear mechanisms in a wide range of tidal interactions, in: *Tidal Hydrodynamics*, B. P. Parker (ed), pp. 237-268, John Wiley, New York

Pattiaratchi, C. B. and Wijeratne, E. M. S., 2009. Tide Gauge Observations of the 2004–2007 Indian Ocean Tsunamis from Sri Lanka and Western Australia. *Pure, Appl. Geophys,* **166**, 233-258.

Rabinovich, A. B., 1997. Spectral analysis of tsunami waves: Separation of source and topography effects. *J. Geophys. Res.*, **102**(C6), 12,663-12,676.

Rabinovich, A. B. and Stephenson, F. E., 2004. Longwave Measurements for the Coast of British Columbia and Improvements to the Tsunami Warning Capability. *Natural Hazards*, **32**, 313-343.

Rabinovich, A. B. and R. E. Thompson, 2007. The 26 December 2004 Sumatra tsunami: Analysis of tide gauge data from the world ocean Part 1. Indian Ocean and South Africa. *Pure Appl. Geophys.*, **164**, 261-308.

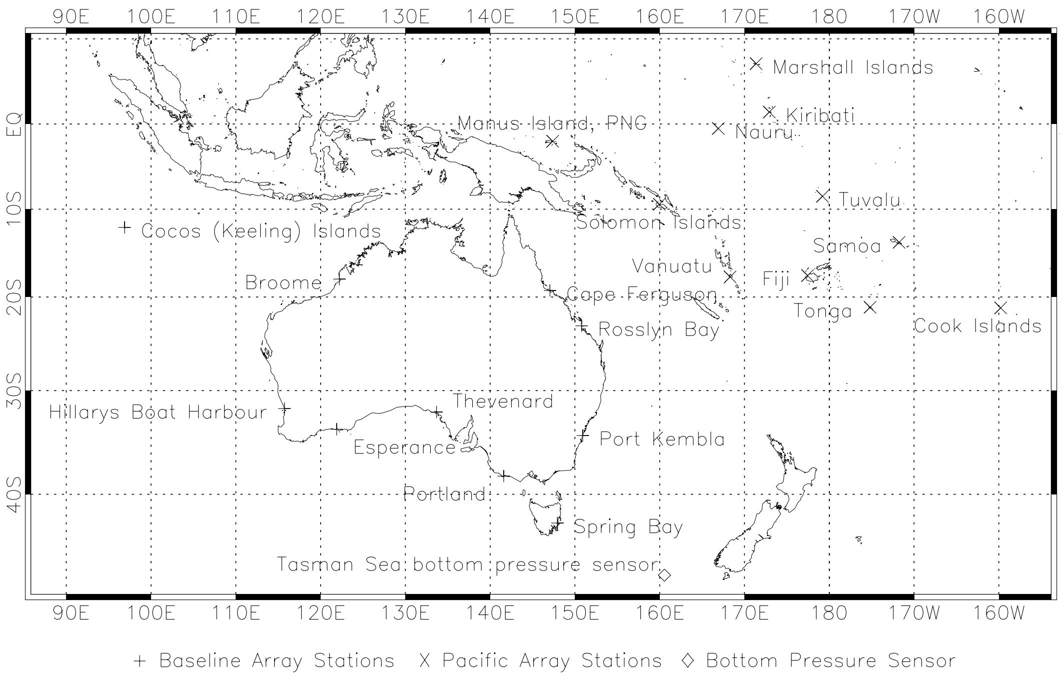

Figure 1: **Location of 'key' baseline tide gauges considered in this study and location of the Australian bottom pressure sensor (tsunameter).**

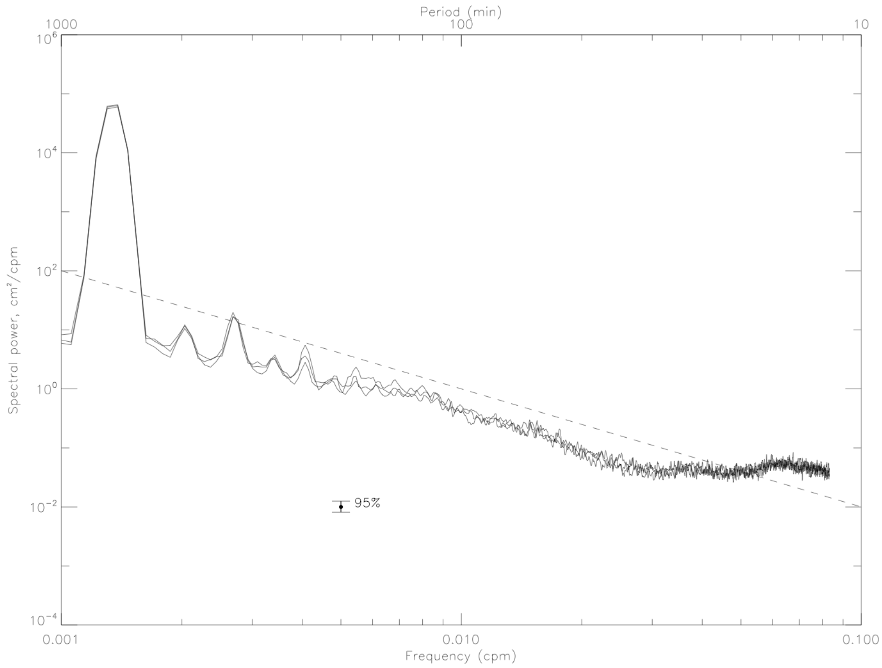

Figure 2: **Yearly power spectra for Cocos Islands' tide gauge for the years 2001, 2002 and 2006. The theoretical deep-water spectrum is represented by the dashed line. Note that the top horizontal axis is not logarithmic in period, but is the inverse of the logarithmic frequency axis. As such, the first tick mark to the right of 1000 minutes is not 900 minutes, but 500 minutes.**

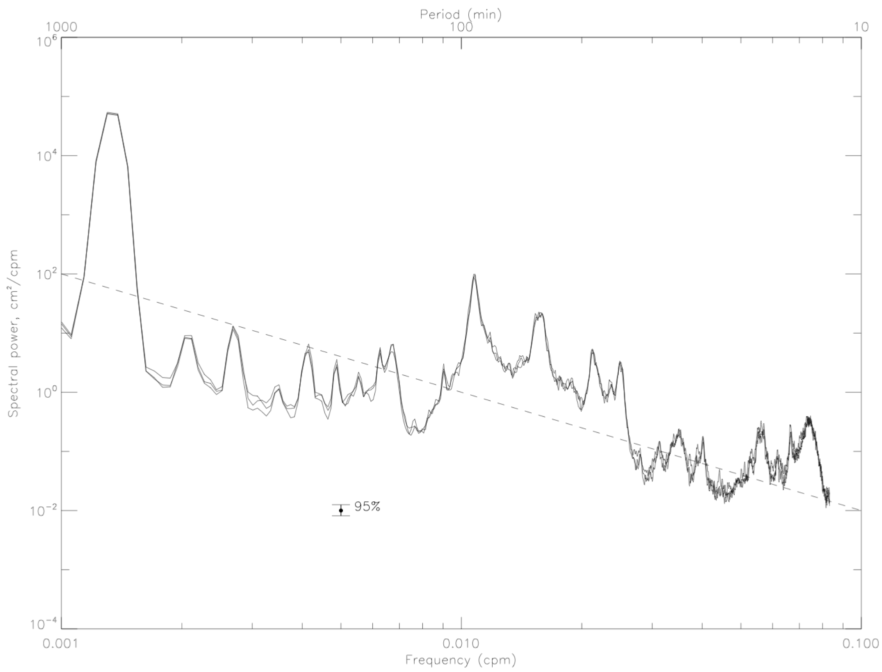

Figure 3: **As for figure 2, but for the Spring Bay tide gauge in Tasmania.**

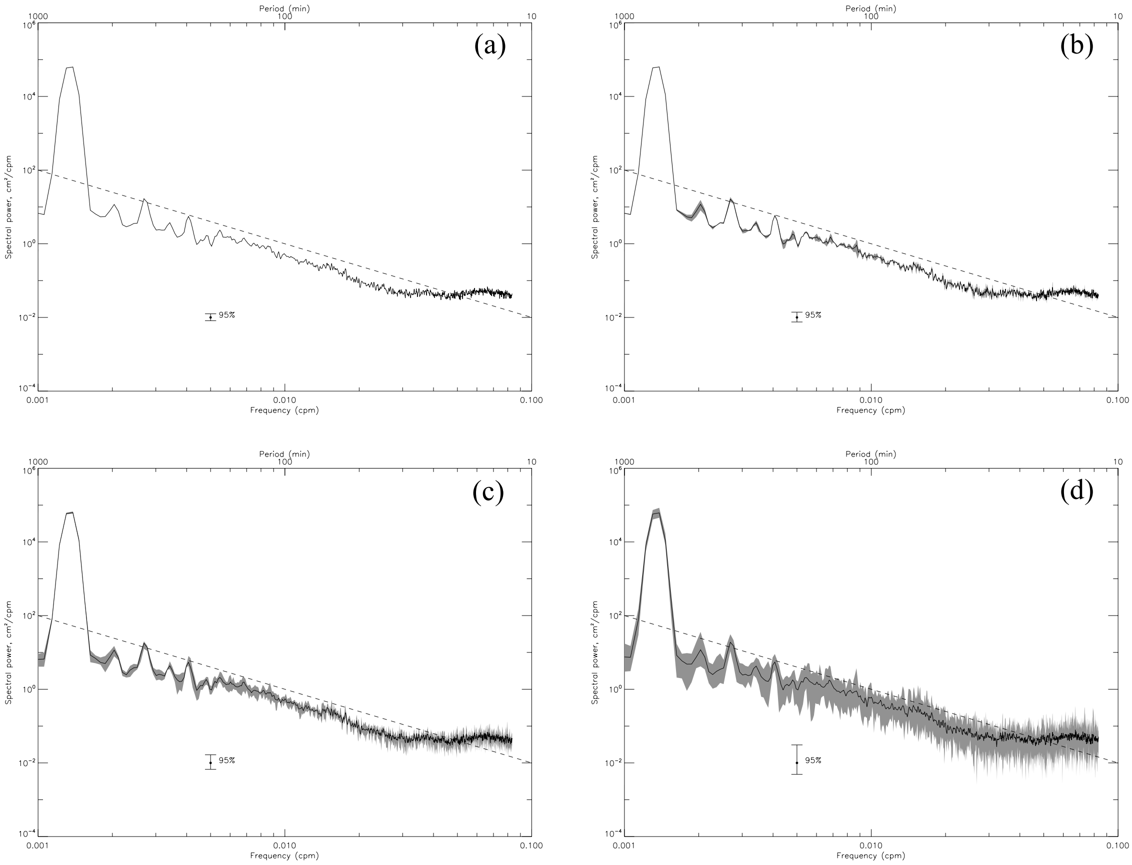

Figure 4: **Power spectra for Cocos Islands, 2002, calculated by splitting the yearly time-series into pieces. The spectra for** (a) **yearly,** (b) **6 monthly,** (c) **3 monthly and** (d) **1 monthly time series are shown. In each, the black curve represents the mean of the spectra and the grey shading represents the total spread of the spectral variability. The theoretical deep-water spectrum is represented by the dashed line.**

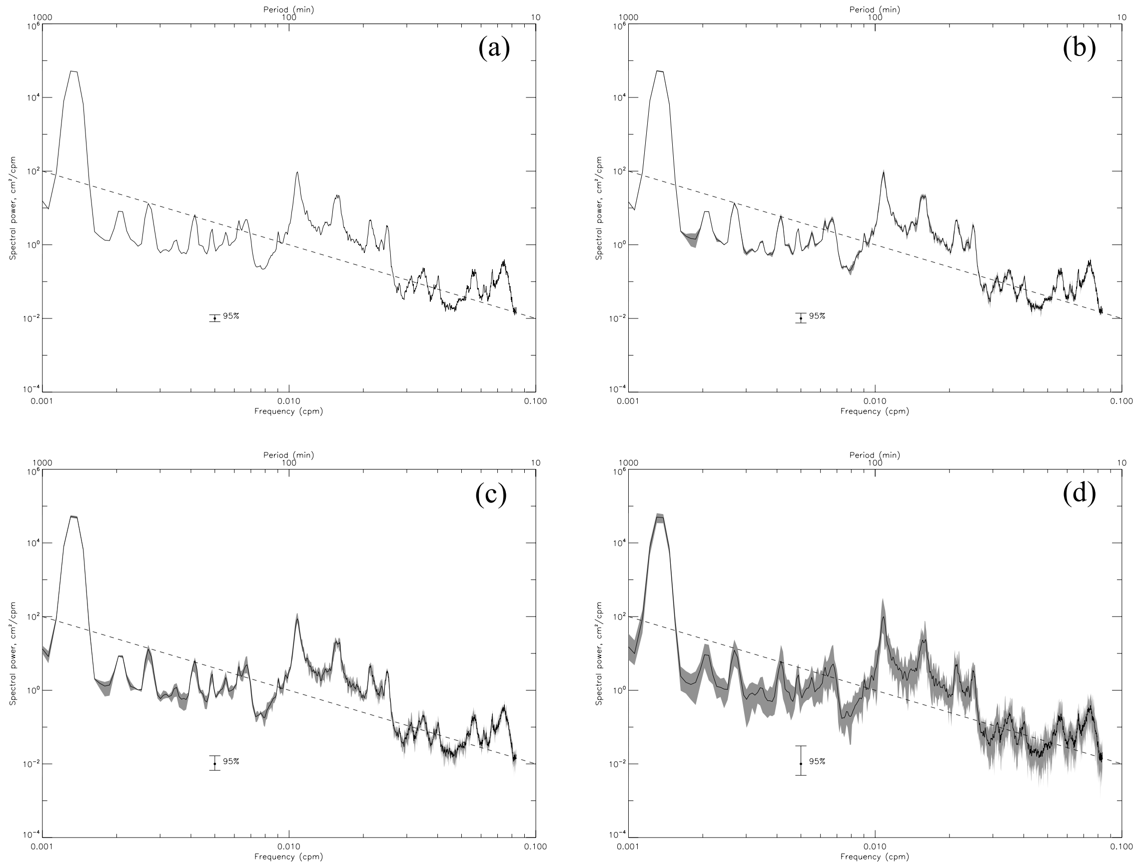

Figure 5: **As for figure 4, but for Spring Bay, Tasmania, 2002.**

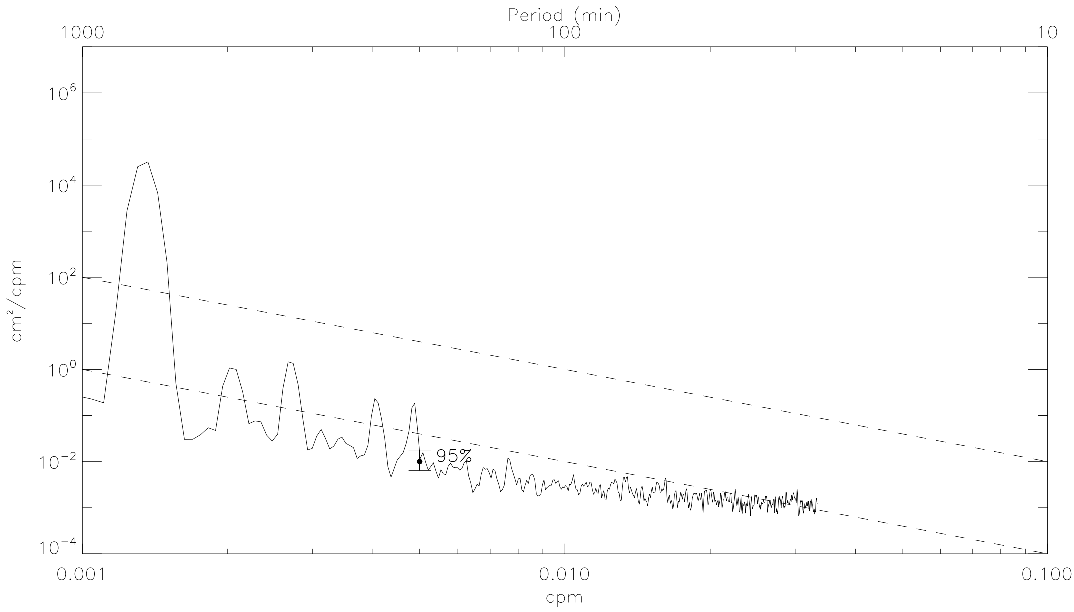

Figure 6: **Power spectrum from bottom pressure sensor 55401 in the Tasman Sea. The sensor is located at approximately (160°33'44" E, 46°55'20" S) in approximately 5000 metres of water. The spectrum was calculated using approximately 94 days of 15-minute observations between June and September 2007. The 95% confidence interval is shown. The dashed lines show curves of the form A_0f^2, with $A_0 = 10^{-4}$ (upper) and $A_0 = 10^{-6}$ (lower).**

a)

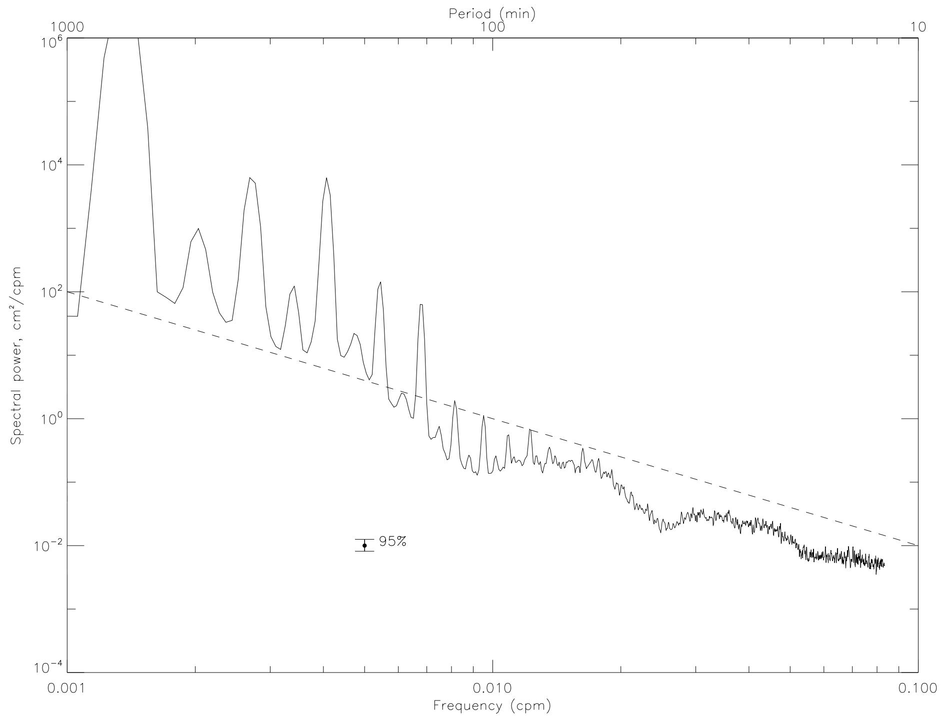

b)

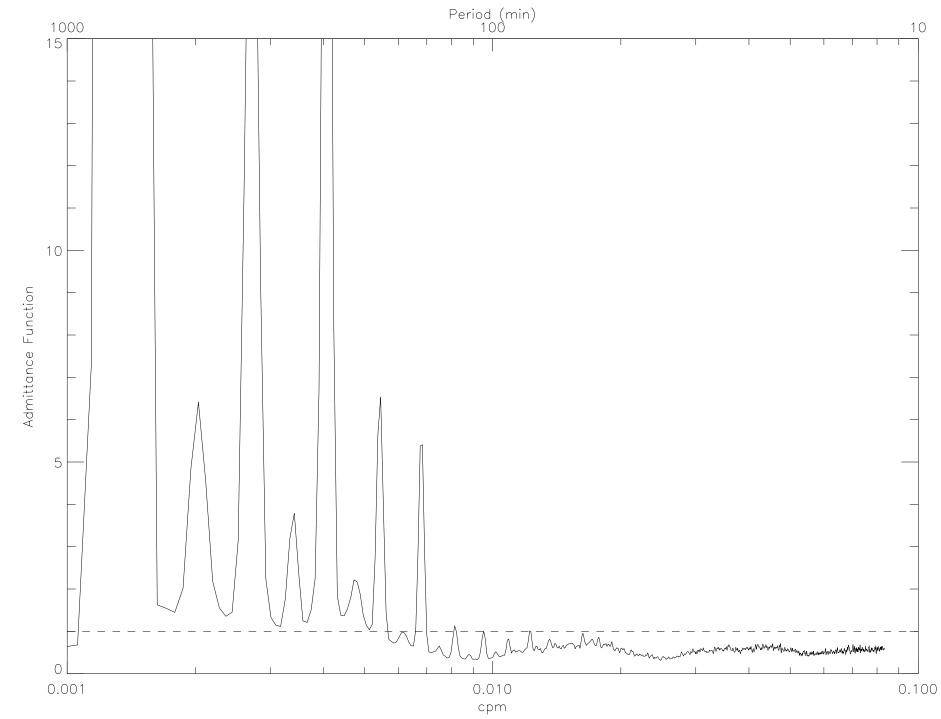

Figure 7: (a) **Power spectrum for Broome, using data from 2002. The 95% confidence interval is indicated and the dashed line represents the hypothetical deep-water spectrum.** (b) **Topographic admittance function determined from the Broome power spectrum.**

a)

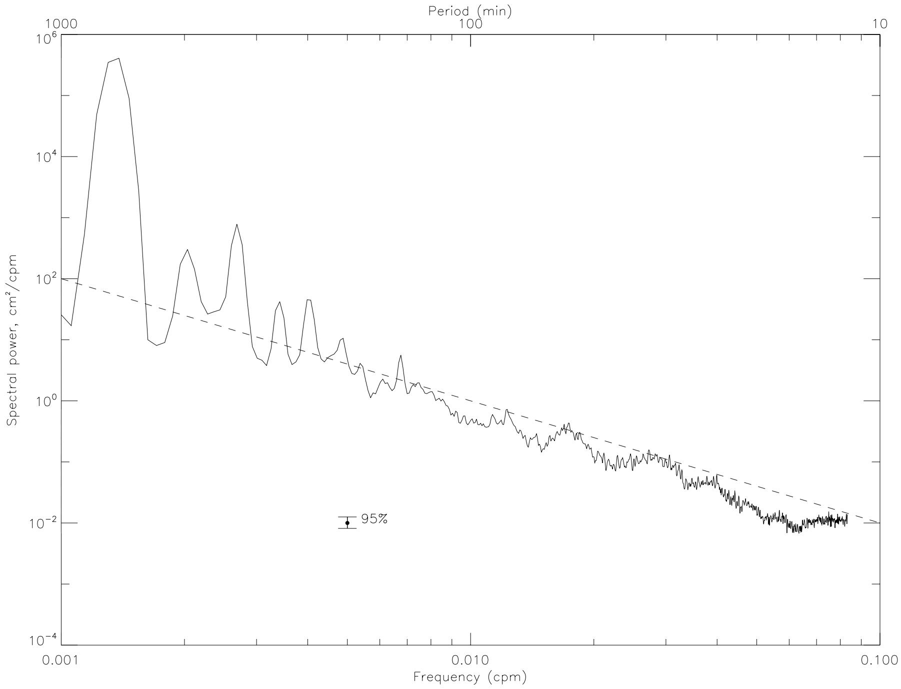

b)

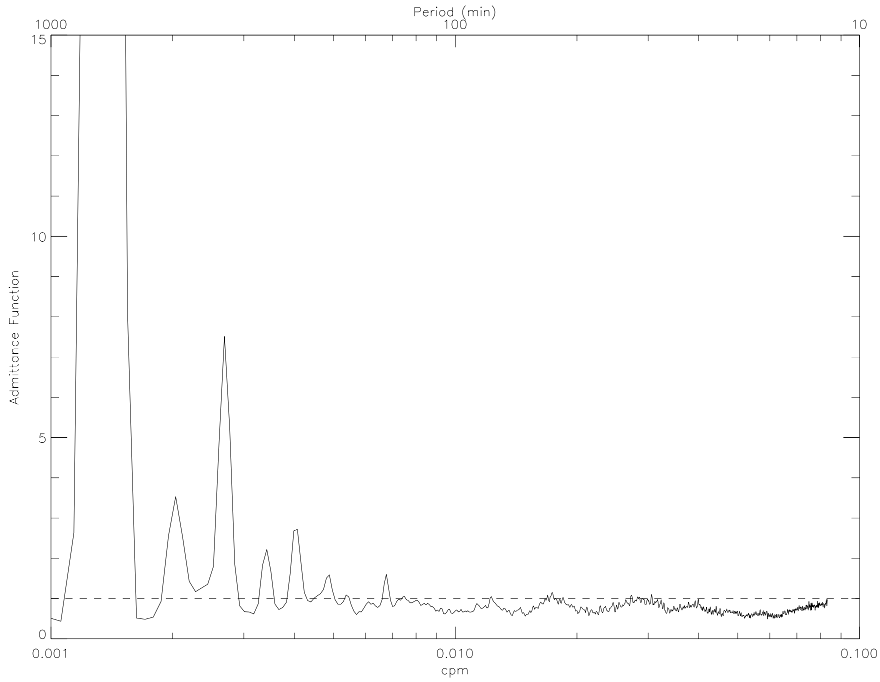

Figure 8: (a) **Power spectrum for Cape Ferguson, using data from 2002. The 95% confidence interval is indicated and the dashed line represents the hypothetical deep-water spectrum.** (b) **Topographic admittance function determined from the Cape Ferguson power spectrum.**

a)

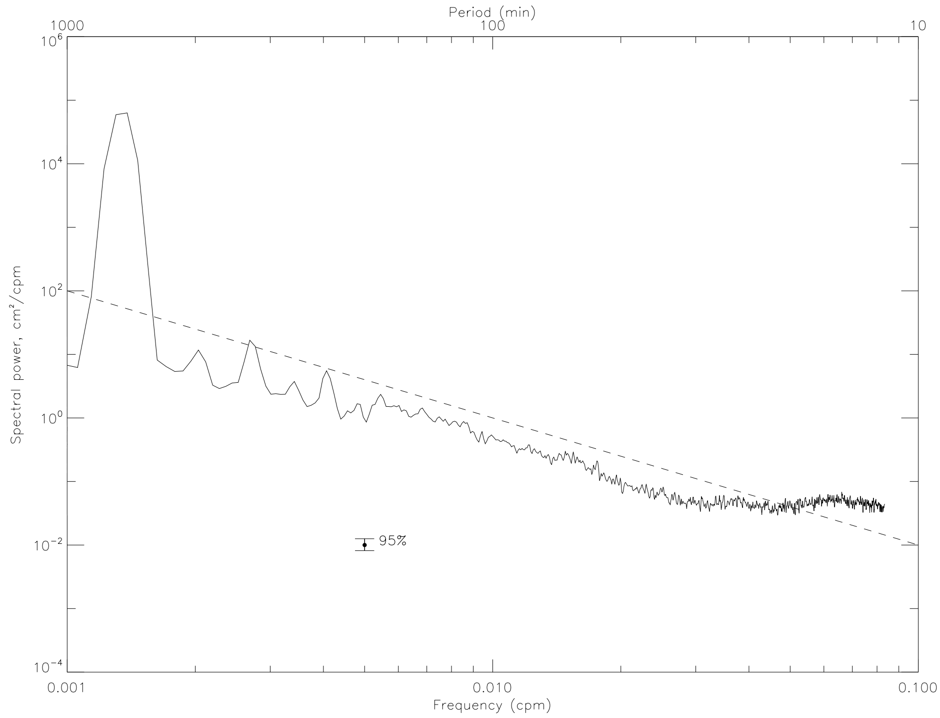

b)

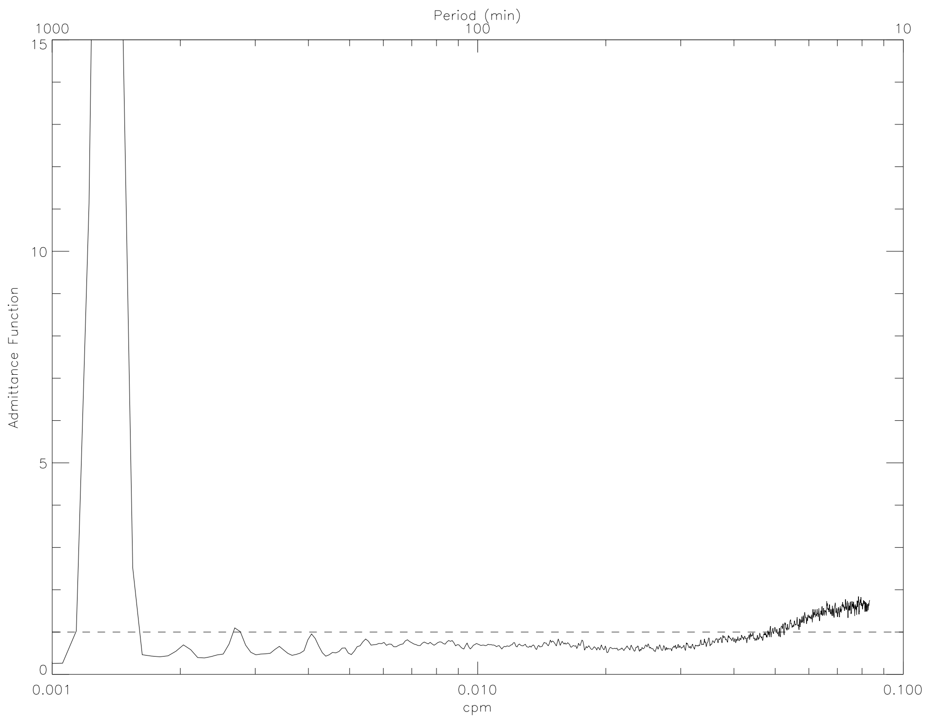

Figure 9: (a) **Power spectrum for Cocos Islands, using data from 2002. The 95% confidence interval is indicated and the dashed line represents the hypothetical deep-water spectrum.** (b) **Topographic admittance function determined from the Cocos Islands power spectrum.**

a)

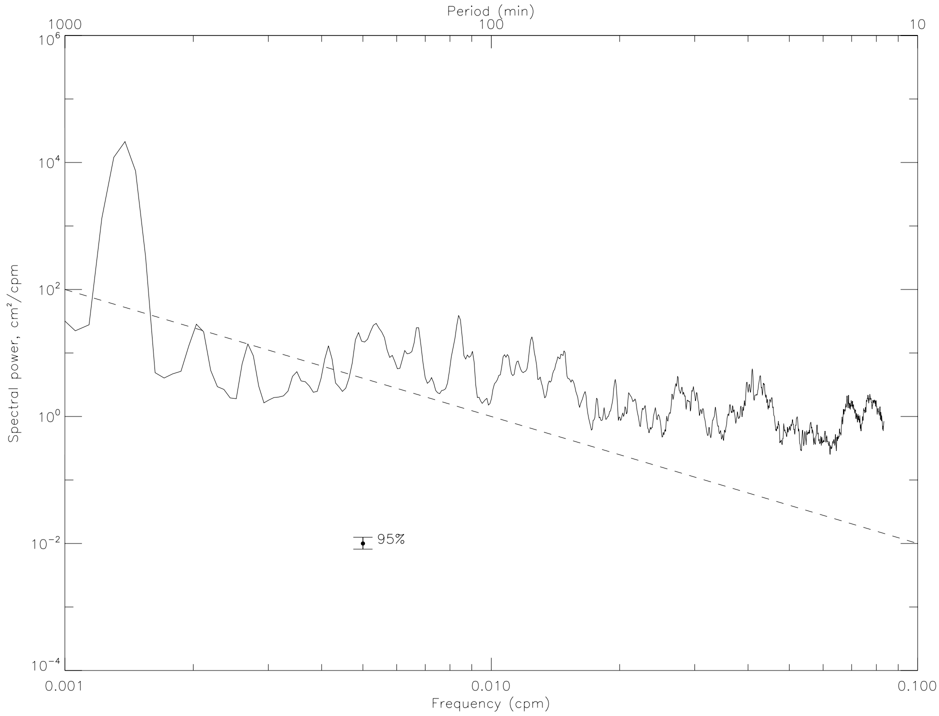

b)

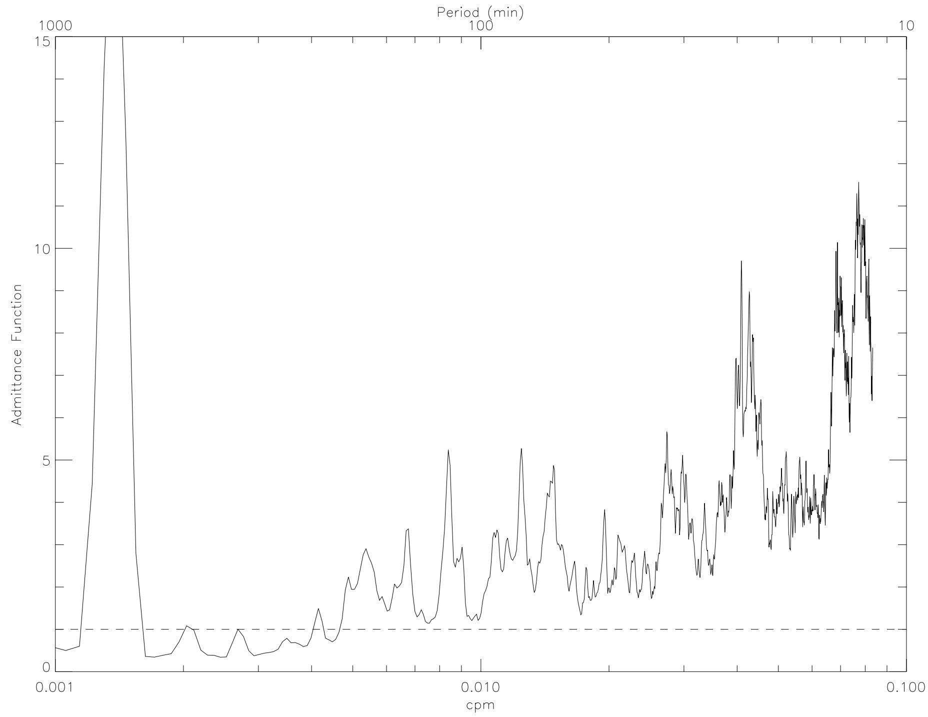

Figure 10: (a) **Power spectrum for Esperance, using data from 2002. The 95% confidence interval is indicated and the dashed line represents the hypothetical deep-water spectrum.** (b) **Topographic admittance function determined from the Esperance power spectrum.**

a)

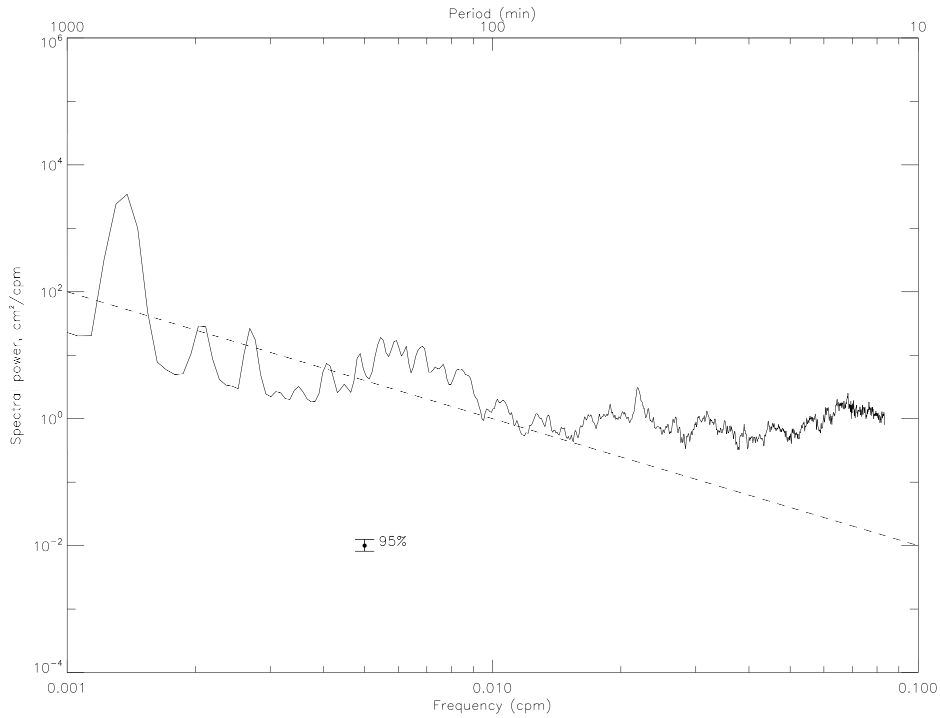

b)

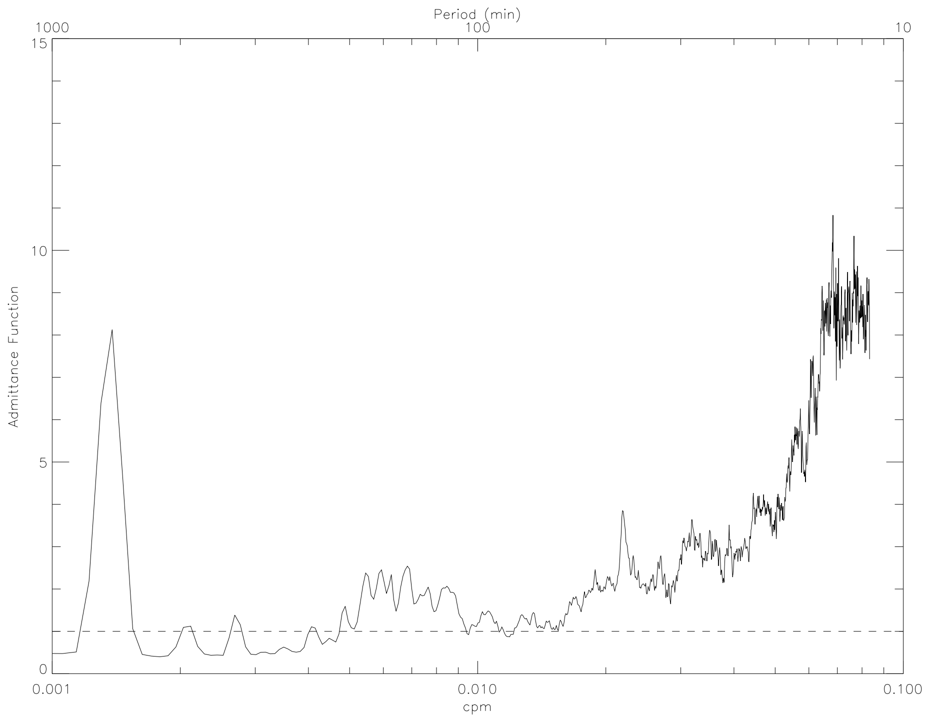

Figure 11: (a) **Power spectrum for Hillarys, using data from 2002. The 95% confidence interval is indicated and the dashed line represents the hypothetical deep-water spectrum.** (b) **Topographic admittance function determined from the Hillarys power spectrum.**

a)

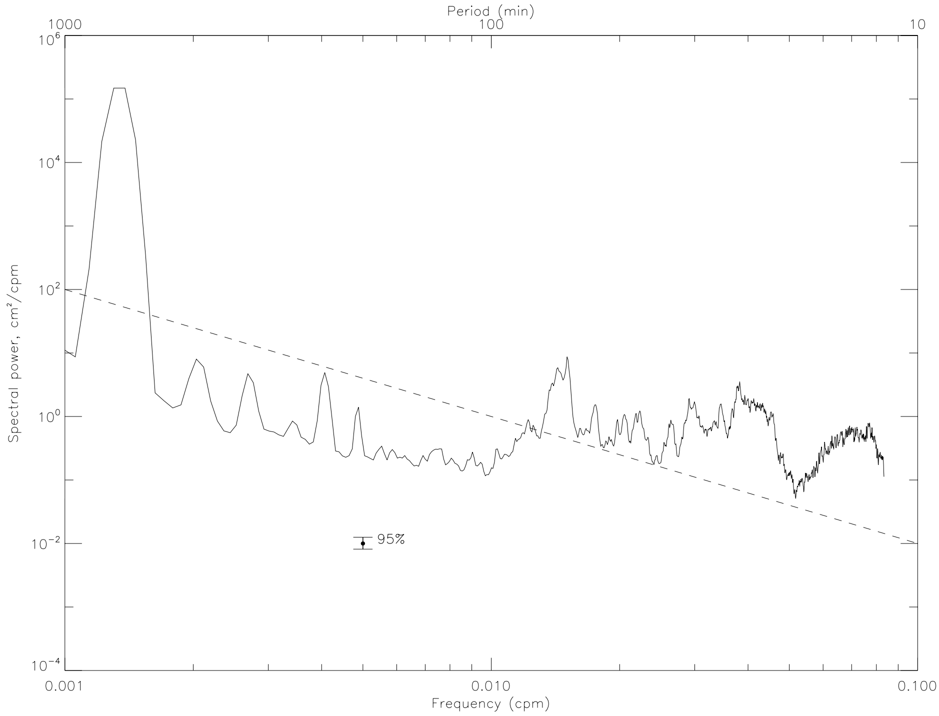

b)

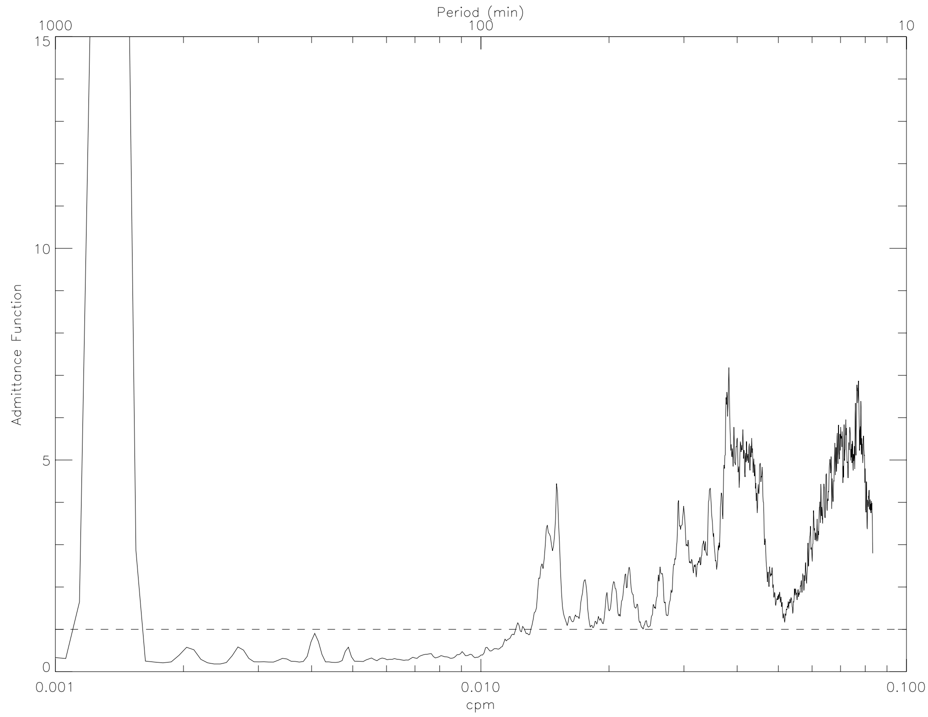

Figure 12: (a) **Power spectrum for Port Kembla, using data from 2002. The 95% confidence interval is indicated and the dashed line represents the hypothetical deep-water spectrum.** (b) **Topographic admittance function determined from the Port Kembla power spectrum.**

a)

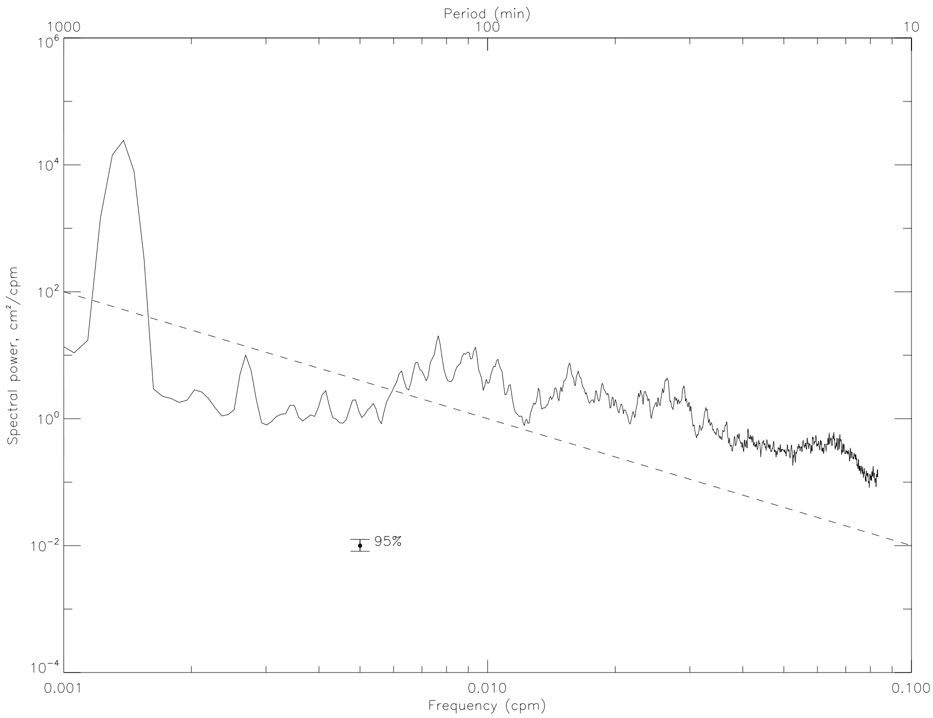

b)

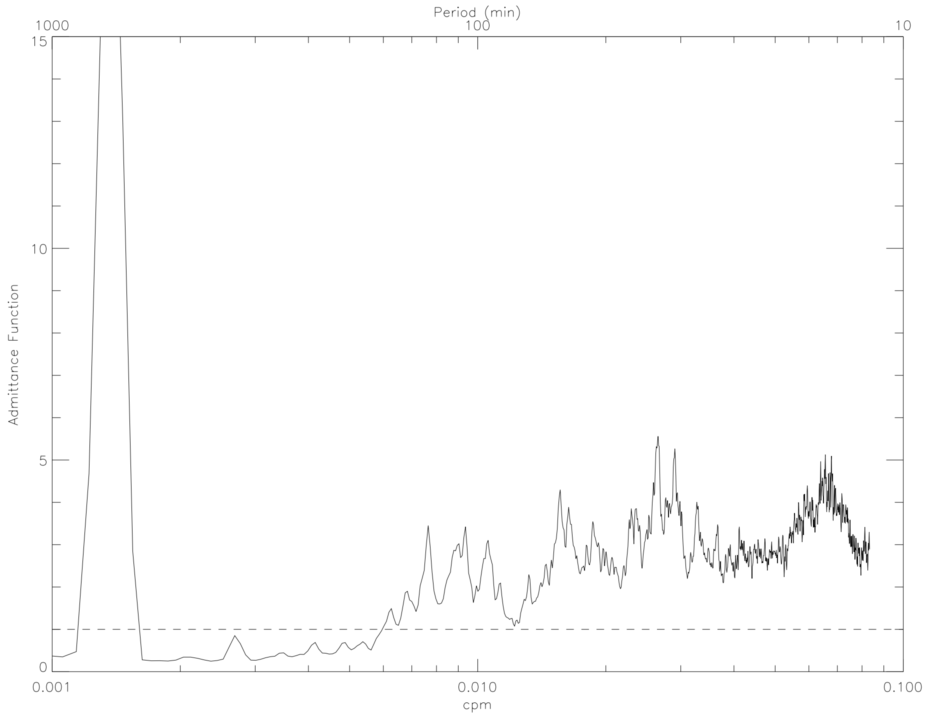

Figure 13: (a) **Power spectrum for Portland, using data from 2002. The 95% confidence interval is indicated and the dashed line represents the hypothetical deep-water spectrum.** (b) **Topographic admittance function determined from the Portland power spectrum.**

a)

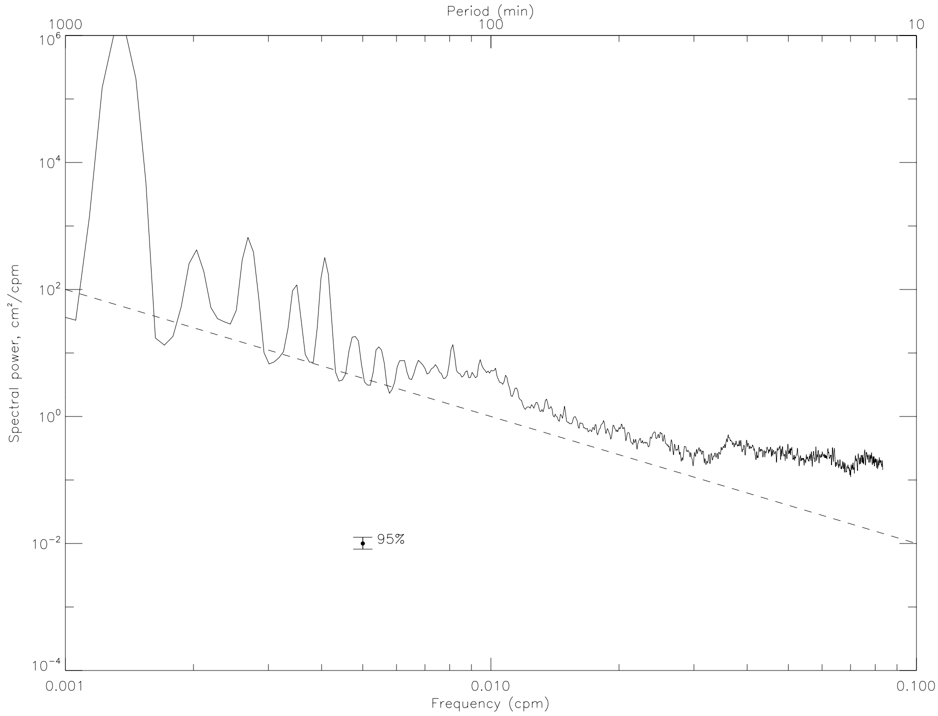

b)

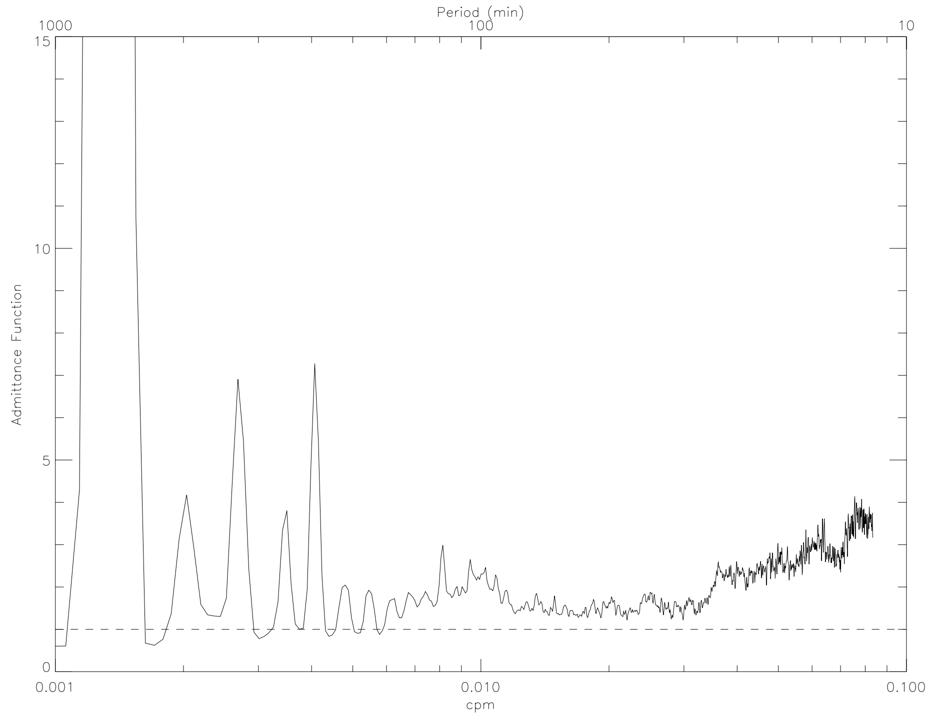

Figure 14: (a) **Power spectrum for Rosslyn Bay, using data from 2002. The 95% confidence interval is indicated and the dashed line represents the hypothetical deep-water spectrum.** (b) **Topographic admittance function determined from the Rosslyn Bay power spectrum.**

a)

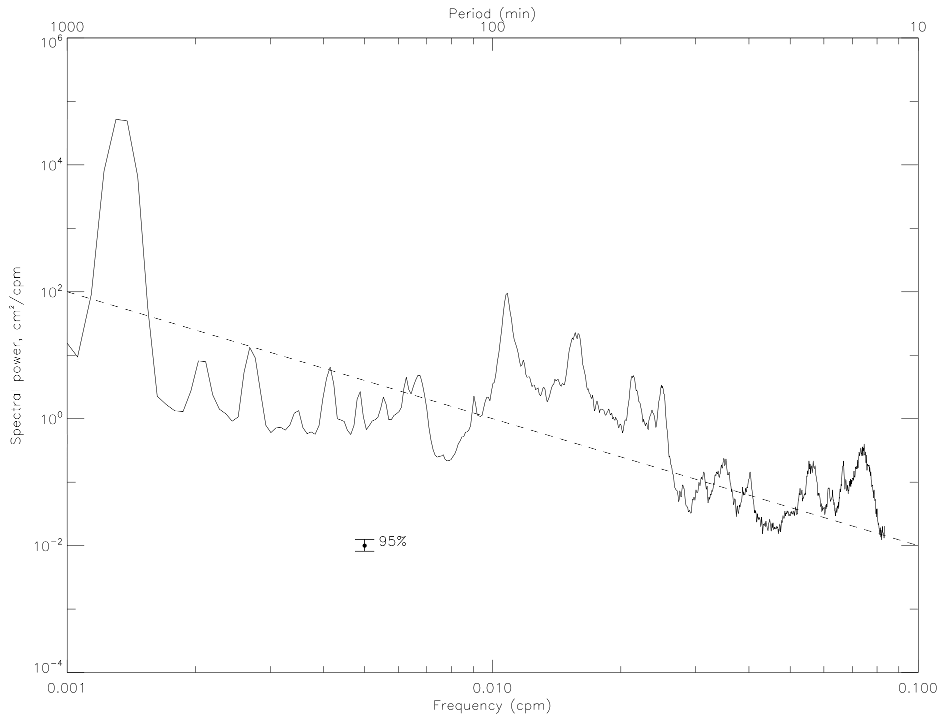

b)

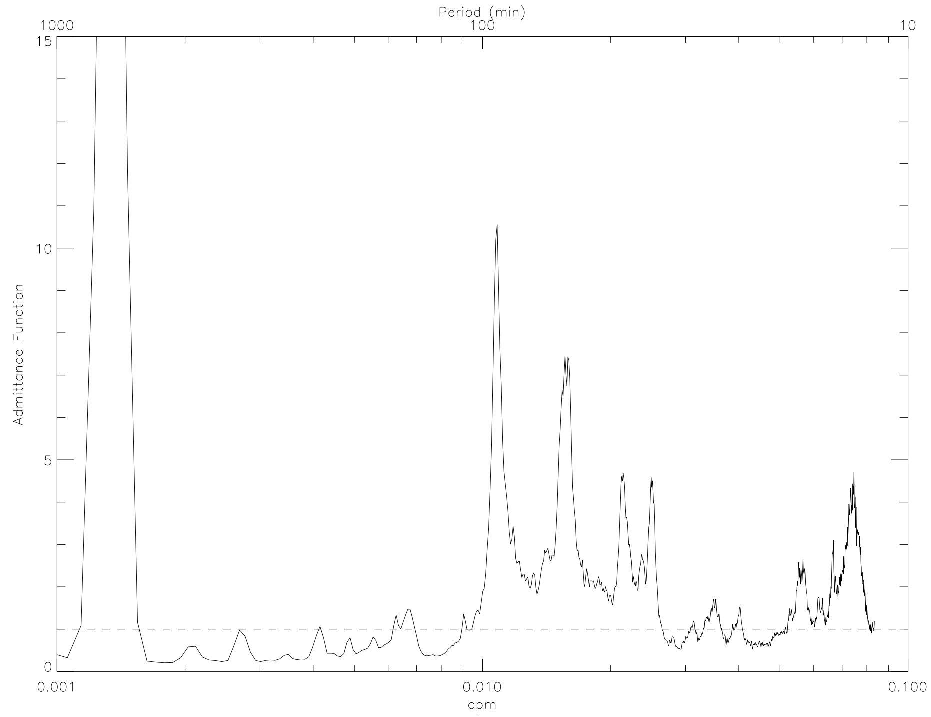

Figure 15: (a) **Power spectrum for Spring Bay, using data from 2002. The 95% confidence interval is indicated and the dashed line represents the hypothetical deep-water spectrum.** (b) **Topographic admittance function determined from the Spring Bay power spectrum.**

a)

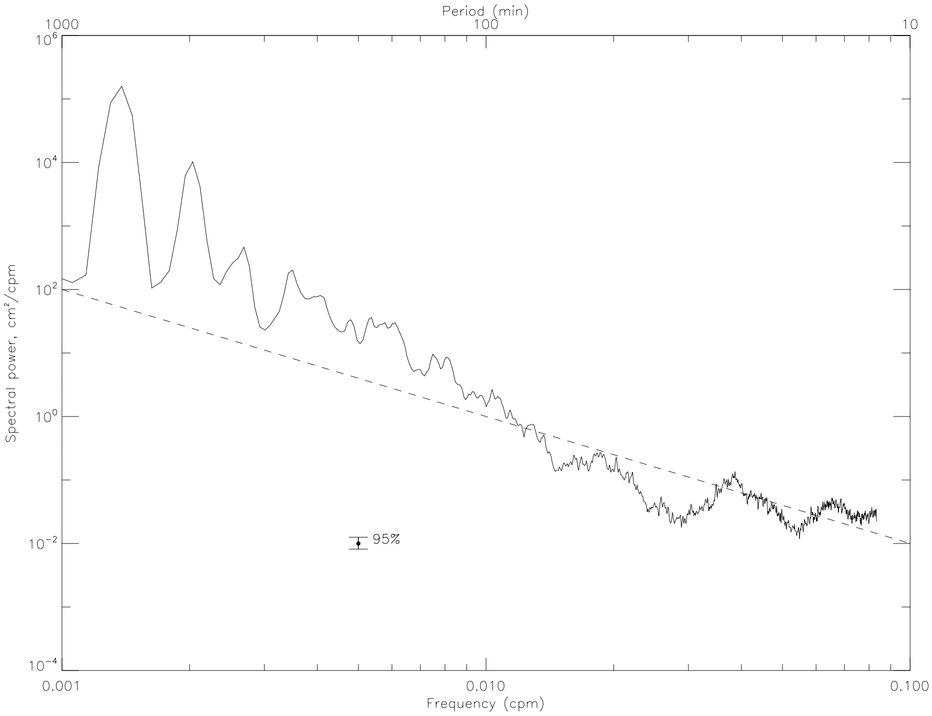

b)

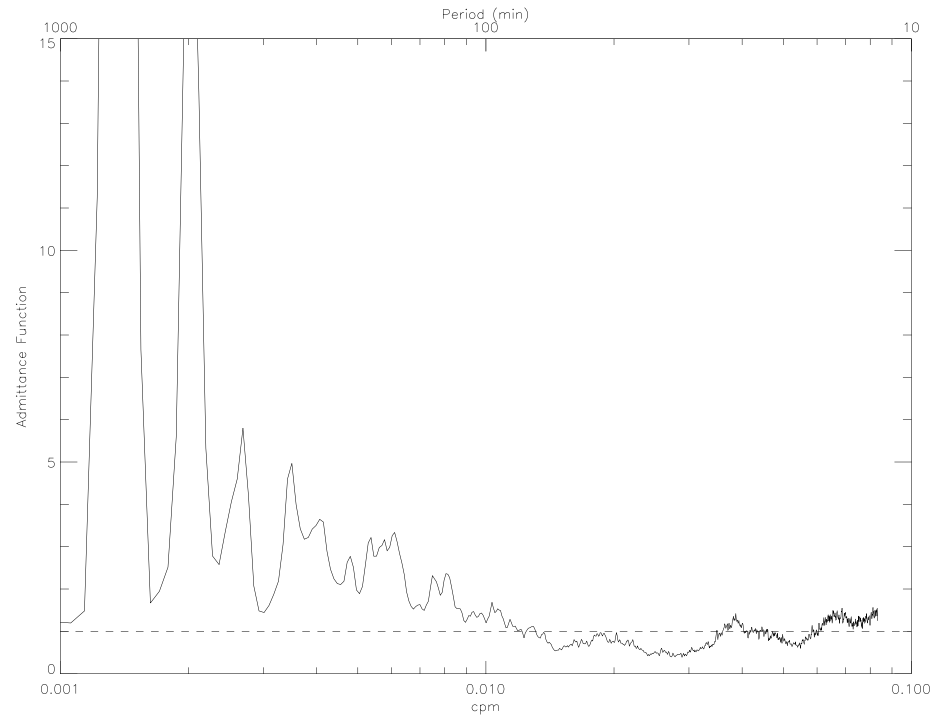

Figure 16: (a) **Power spectrum for Thevenard, using data from 2002. The 95% confidence interval is indicated and the dashed line represents the hypothetical deep-water spectrum.** (b) **Topographic admittance function determined from the Thevenard power spectrum.**

a)

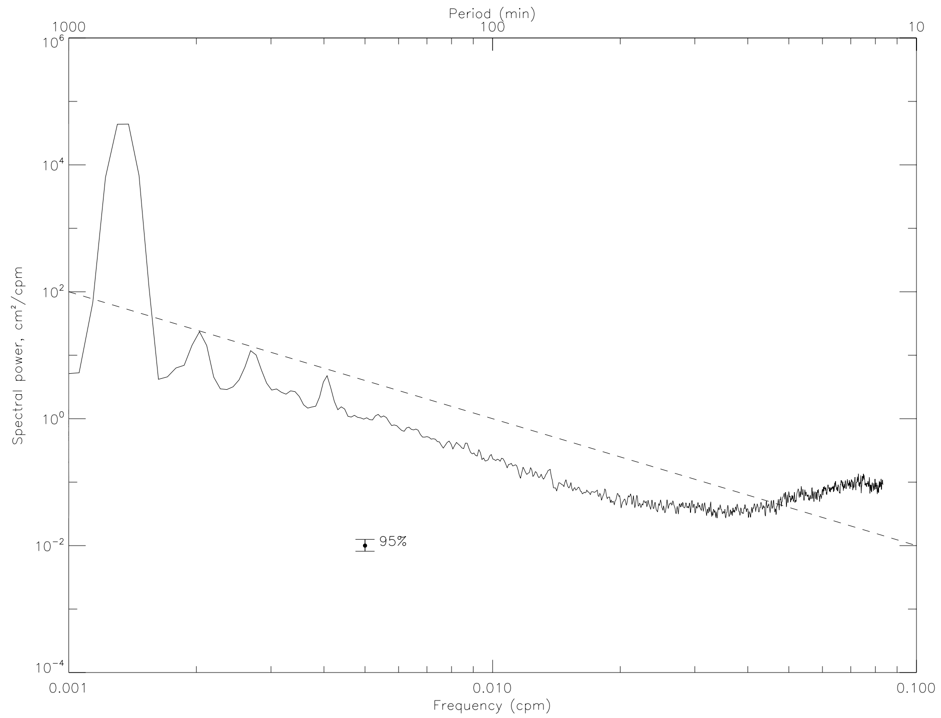

b)

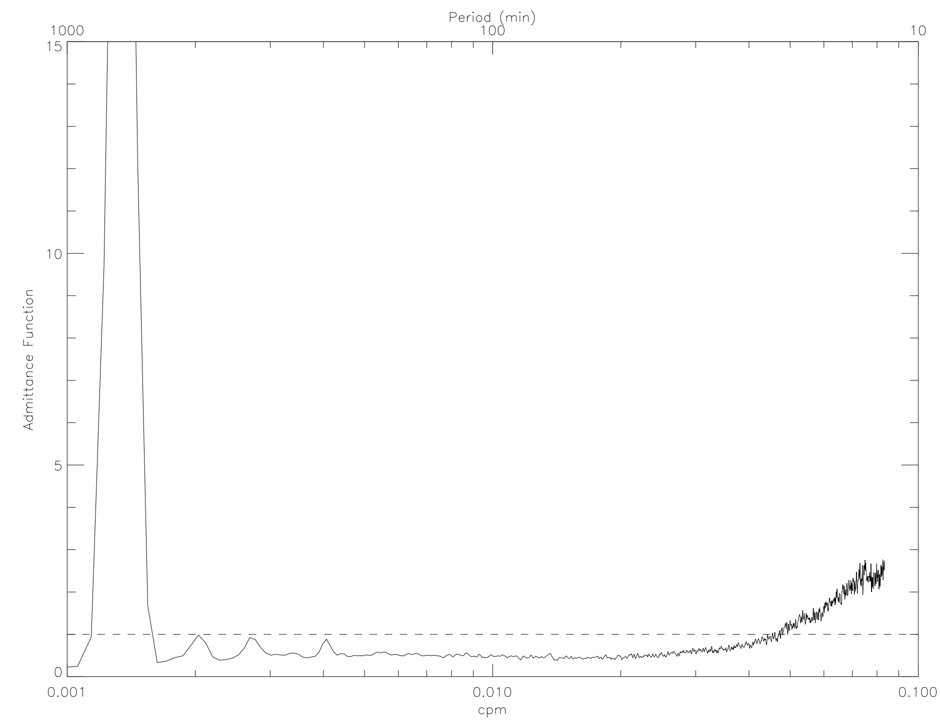

Figure 17: (a) **Power spectrum for Raratonga, the Cook Islands, using data from 2002. The 95% confidence interval is indicated and the dashed line represents the hypothetical deep-water spectrum.** (b) **Topographic admittance function determined from the Raratonga power spectrum.**

a)

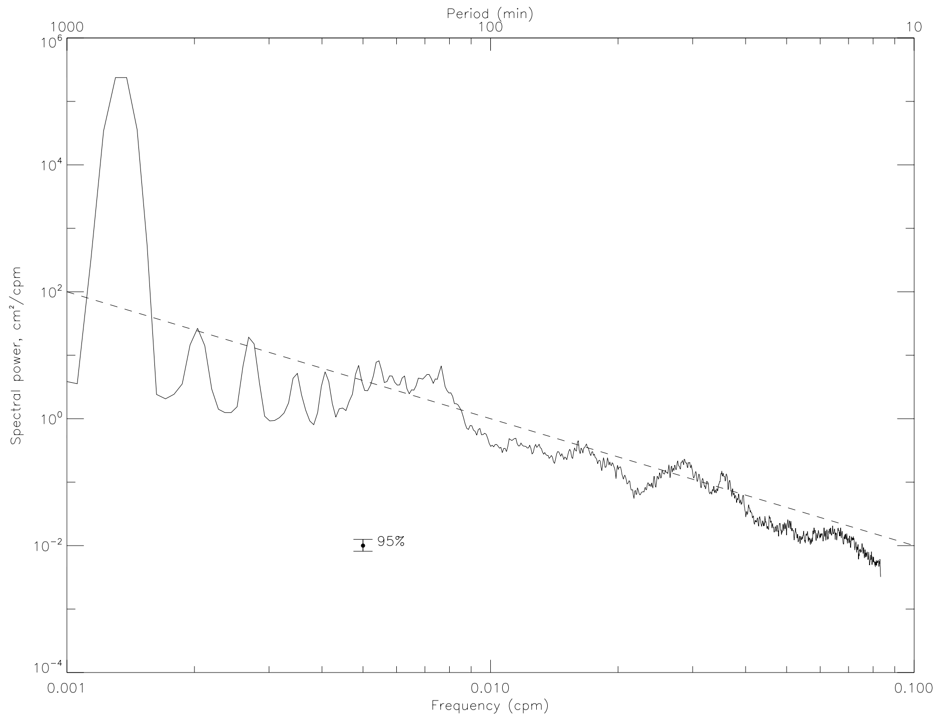

b)

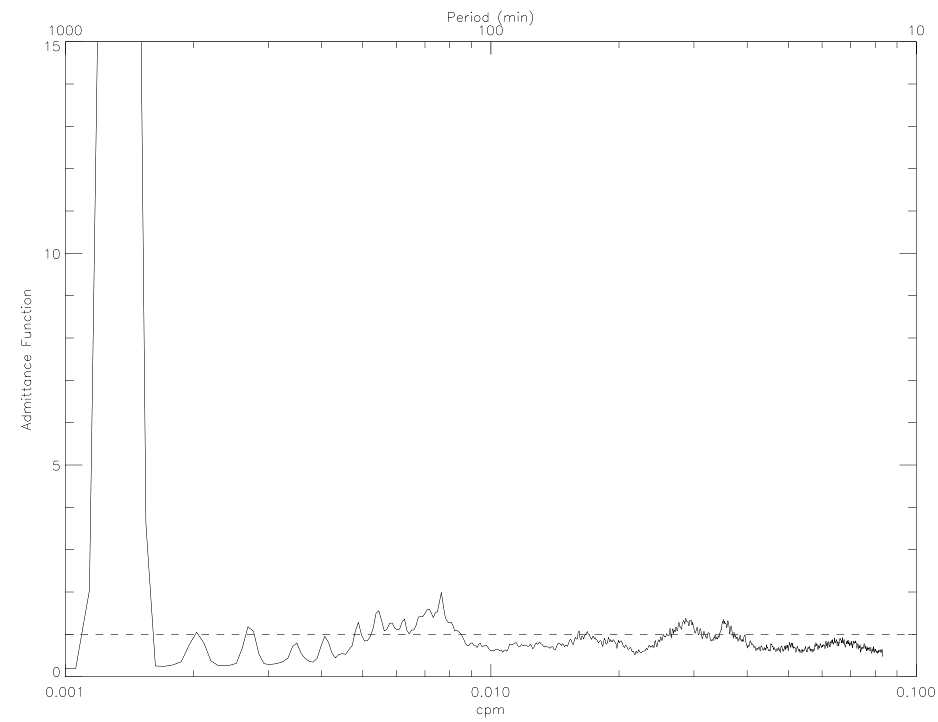

Figure 18: (a) **Power spectrum for Lautoka, Fiji, using data from 2002. The 95% confidence interval is indicated and the dashed line represents the hypothetical deep-water spectrum.** (b) **Topographic admittance function determined from the Lautoka power spectrum.**

a)

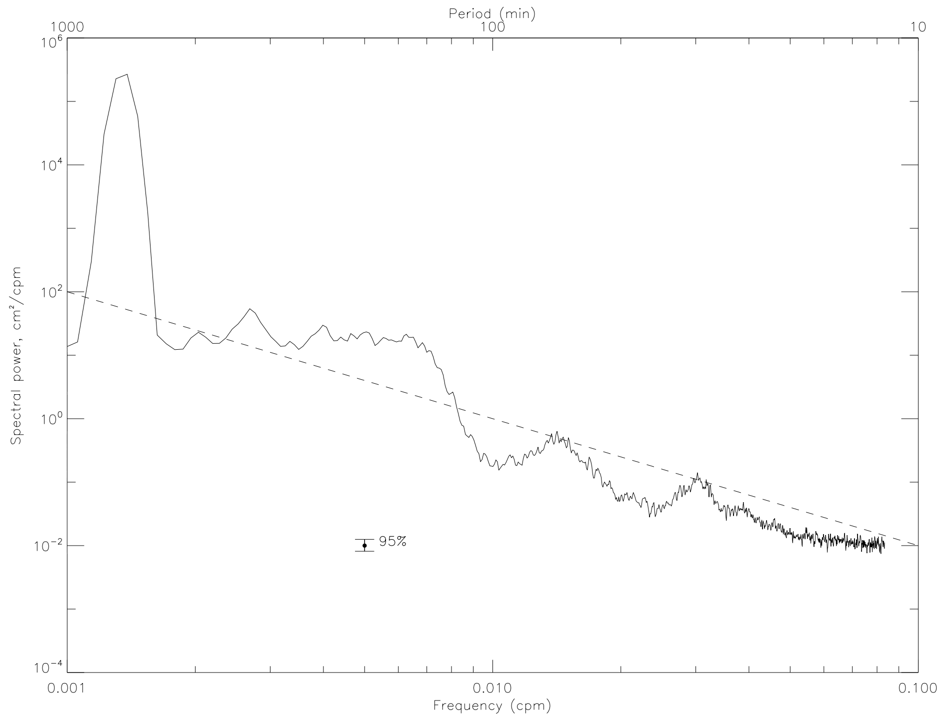

b)

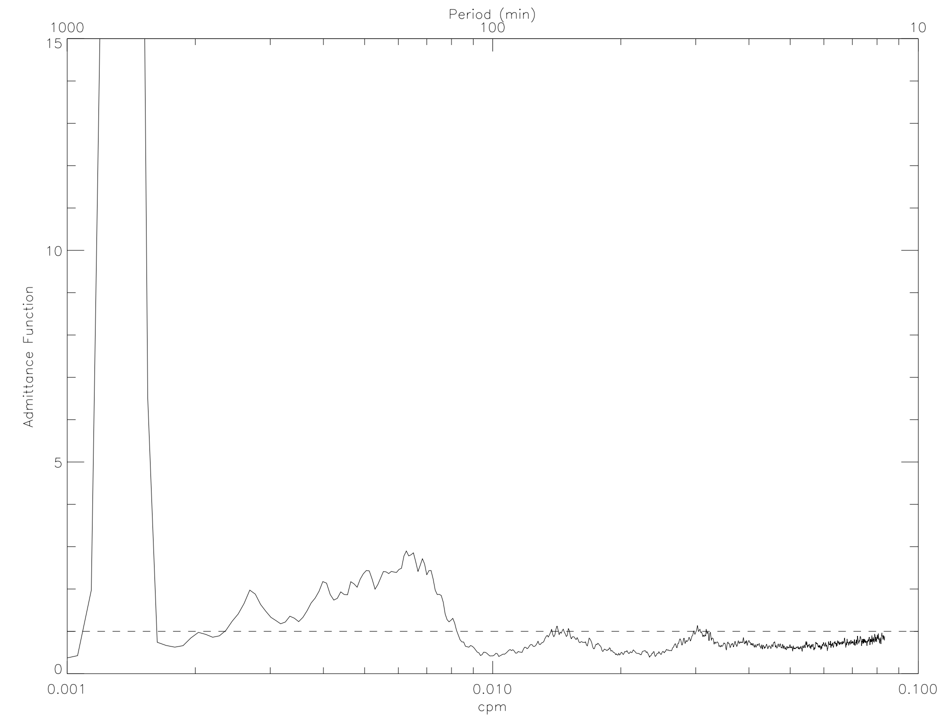

Figure 19: (a) **Power spectrum for Kiribati, using data from 2002. The 95% confidence interval is indicated and the dashed line represents the hypothetical deep-water spectrum.** (b) **Topographic admittance function determined from the Kiribati power spectrum.**

a)

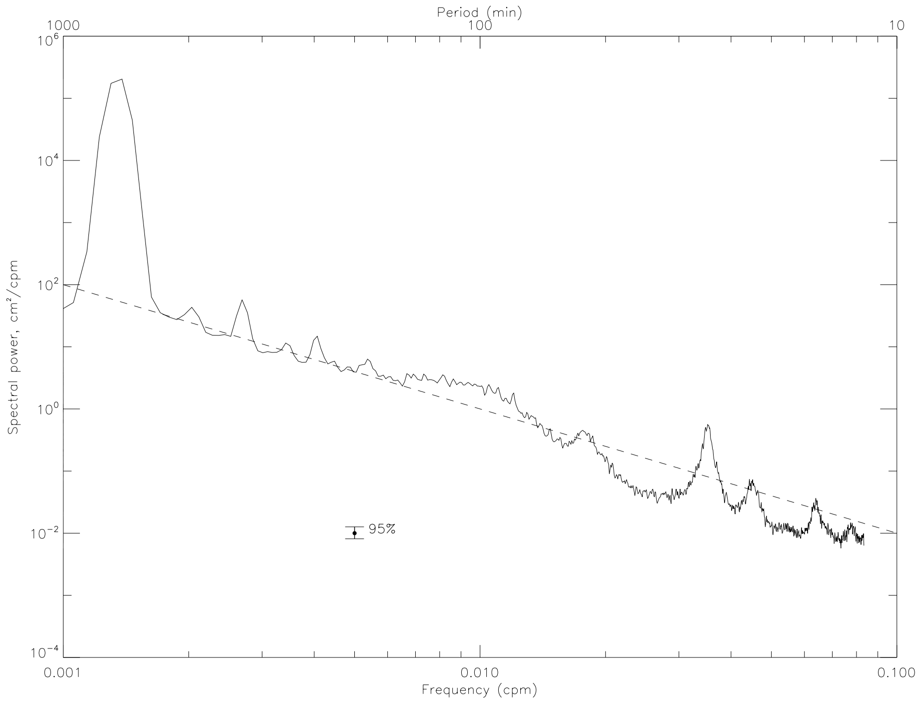

b)

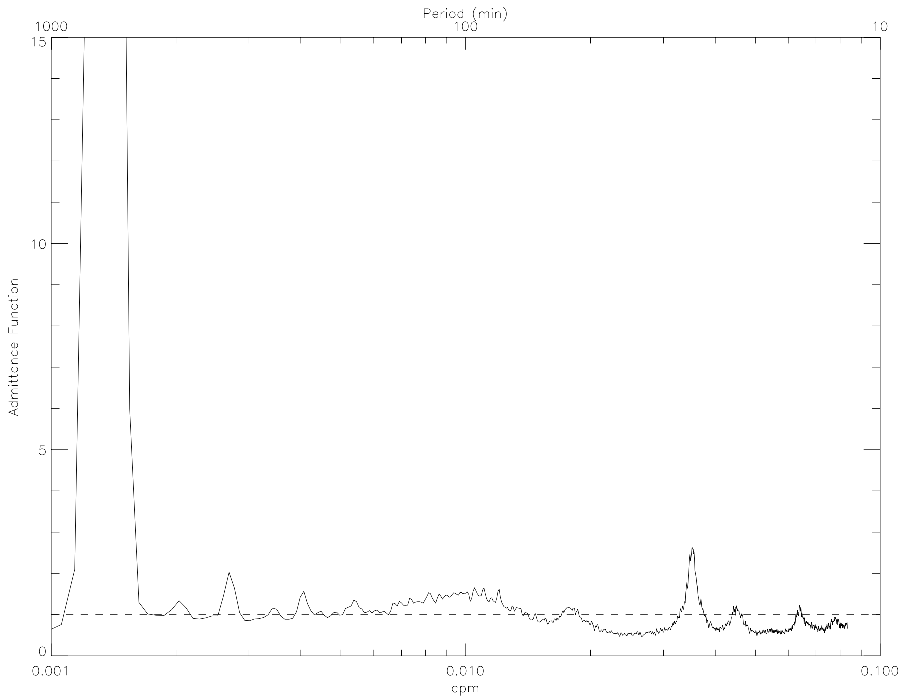

Figure 20: (a) **Power spectrum for the Marshall Islands, using data from 1 January to 1 September, 2002. The 95% confidence interval is indicated and the dashed line represents the hypothetical deep-water spectrum.** (b) **Topographic admittance function determined from the Marshall Islands power spectrum.**

a)

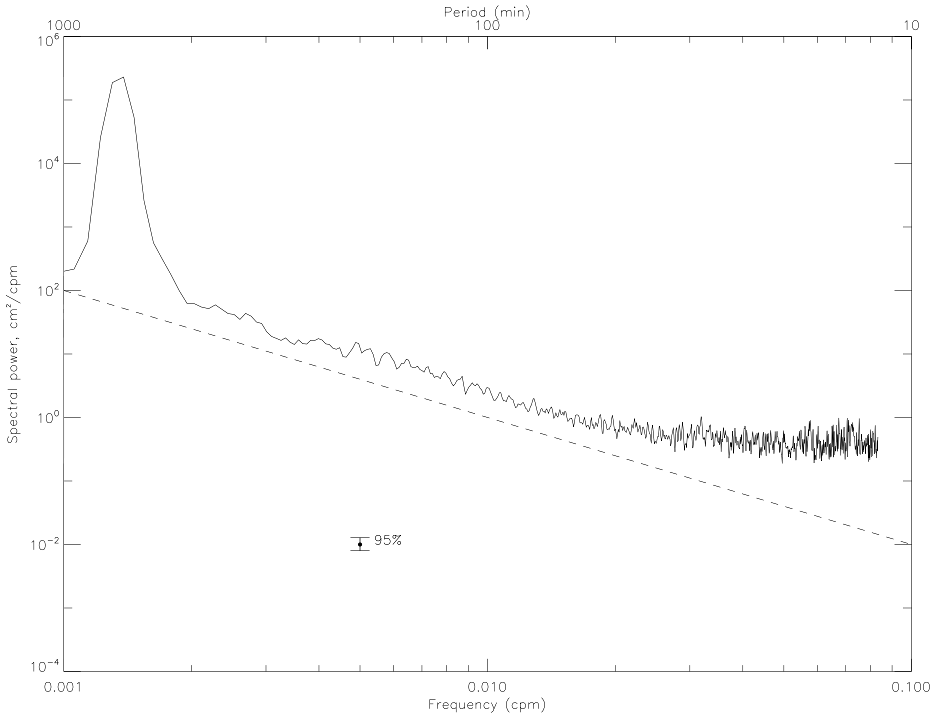

b)

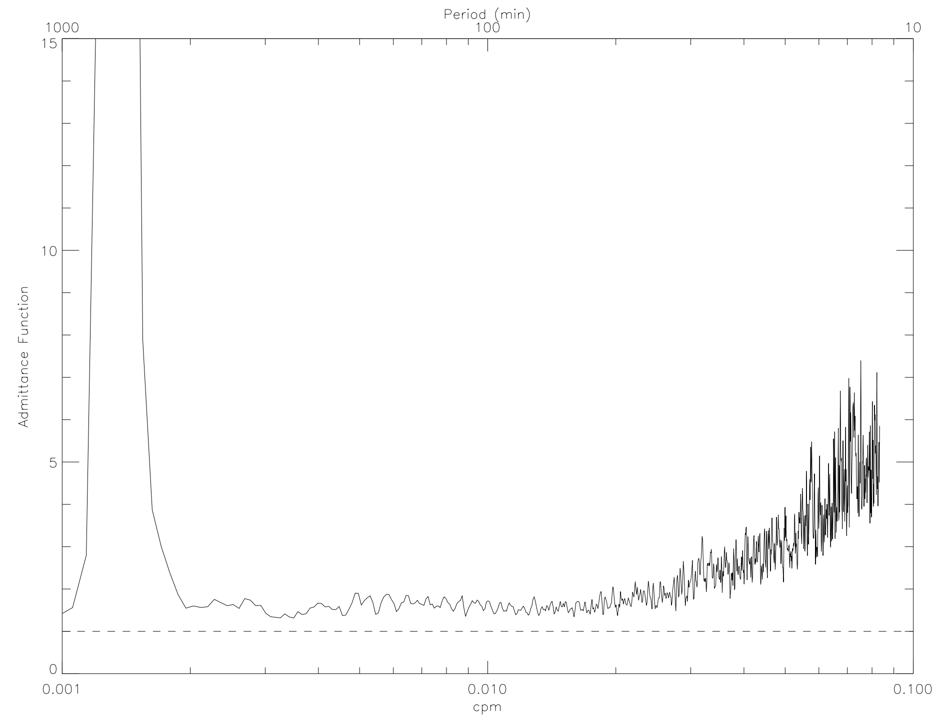

Figure 21: (a) **Power spectrum for Nauru, using data from 1 May to 31 December, 2002. The 95% confidence interval is indicated and the dashed line represents the hypothetical deep-water spectrum.** (b) **Topographic admittance function determined from the Nauru power spectrum.**

a)

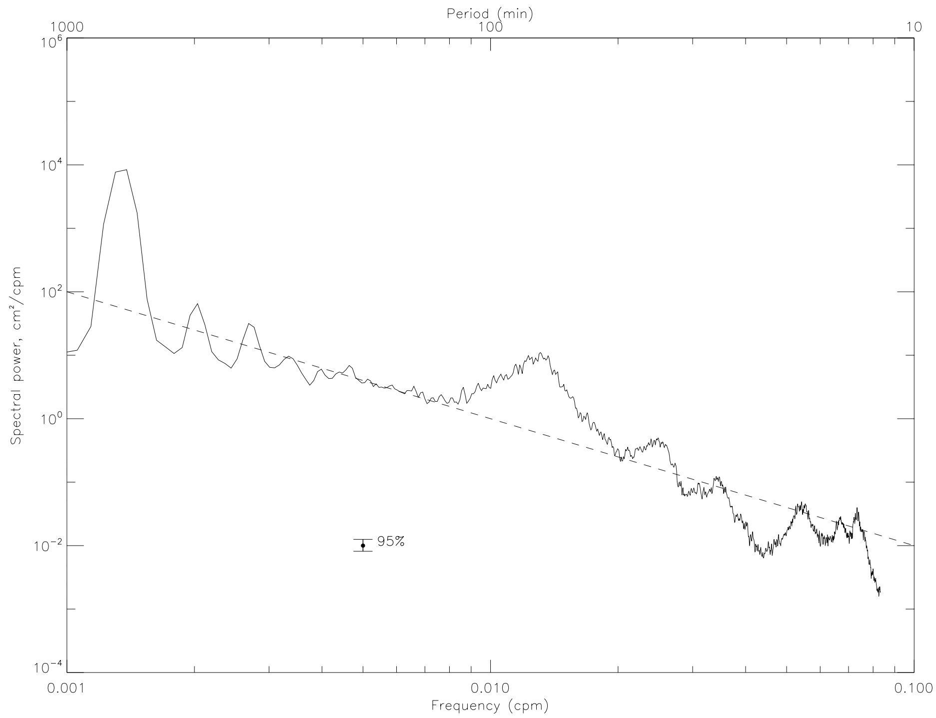

b)

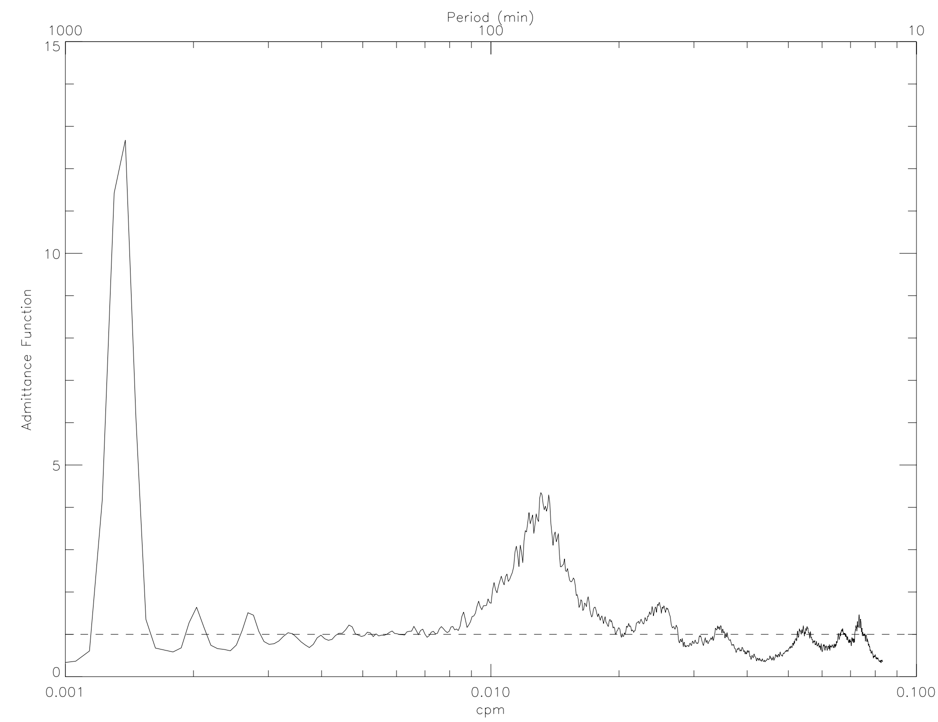

Figure 22: (a) **Power spectrum for Manus Island (PNG), using data from 2002. The 95% confidence interval is indicated and the dashed line represents the hypothetical deep-water spectrum.** (b) **Topographic admittance function determined from the Manus Island power spectrum.**

a)

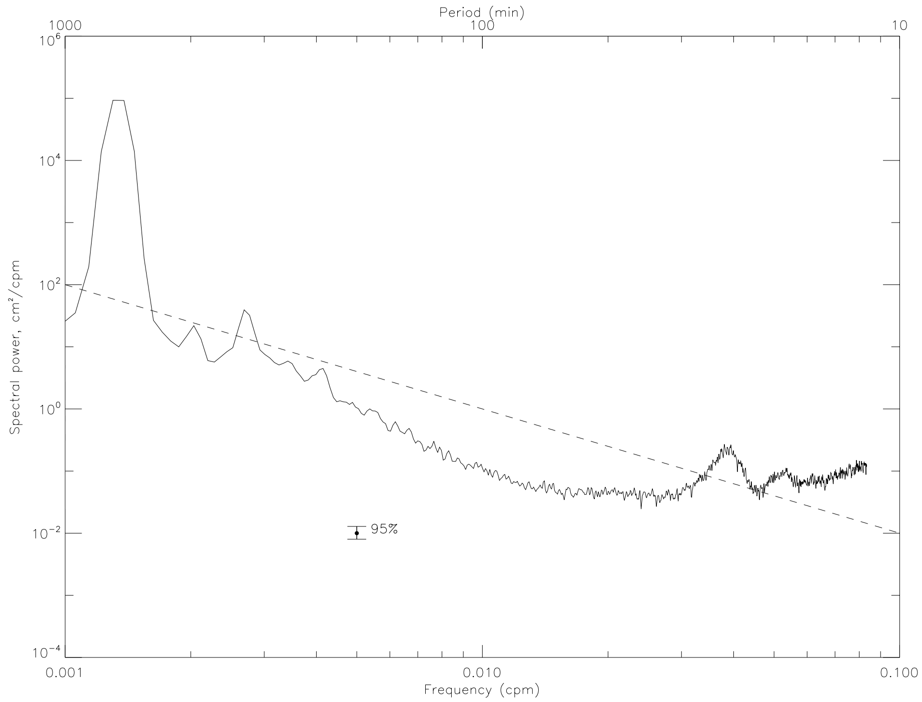

b)

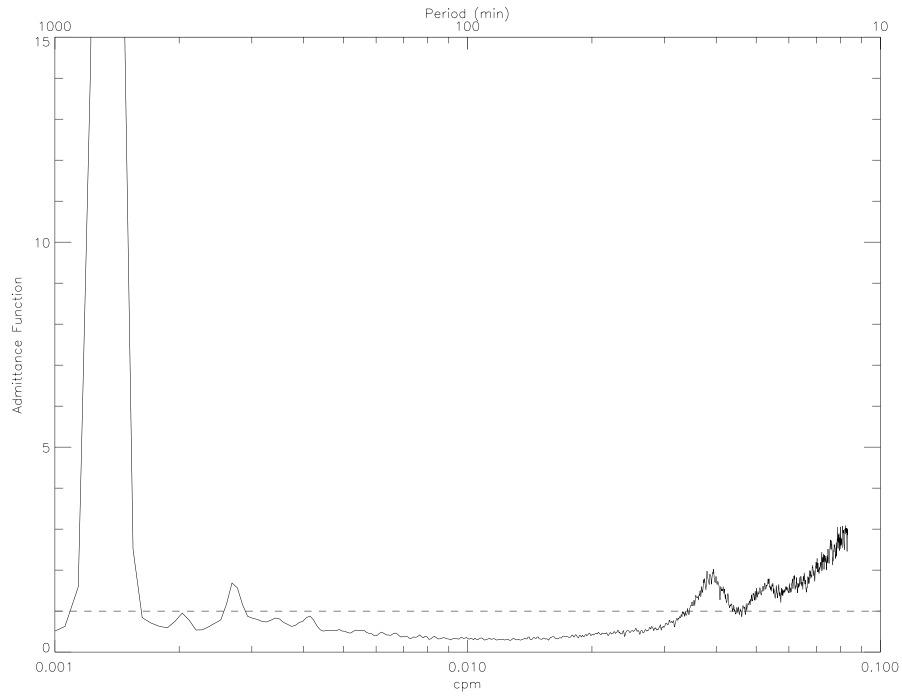

Figure 23: (a) **Power spectrum for Samoa, using data from 1 January to 1 October, 2002. The 95% confidence interval is indicated and the dashed line represents the hypothetical deep-water spectrum.** (b) **Topographic admittance function determined from the Western Samoa power spectrum.**

a)

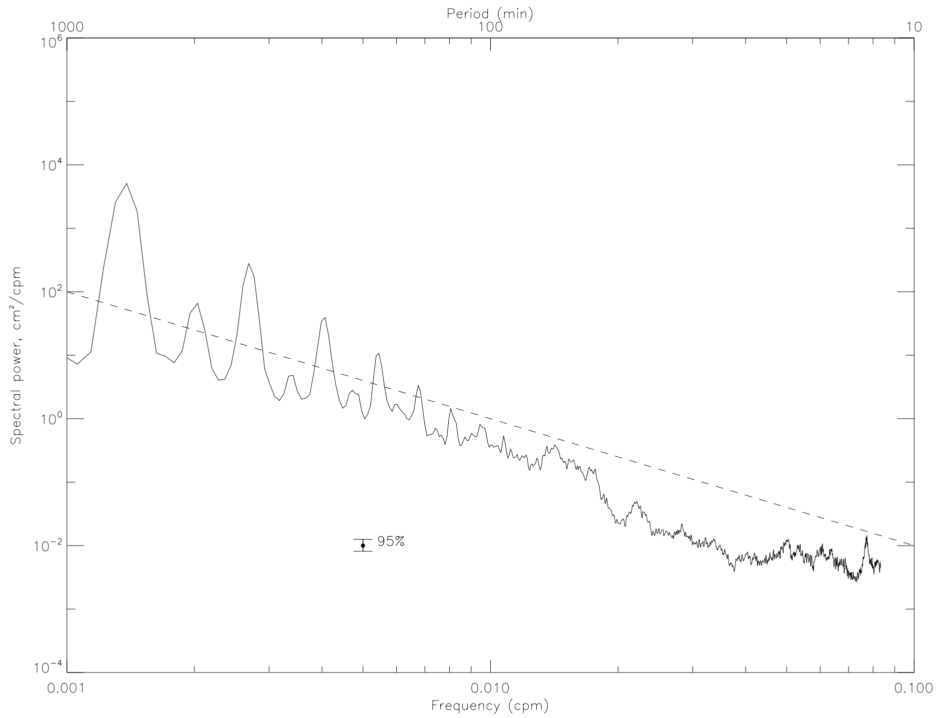

b)

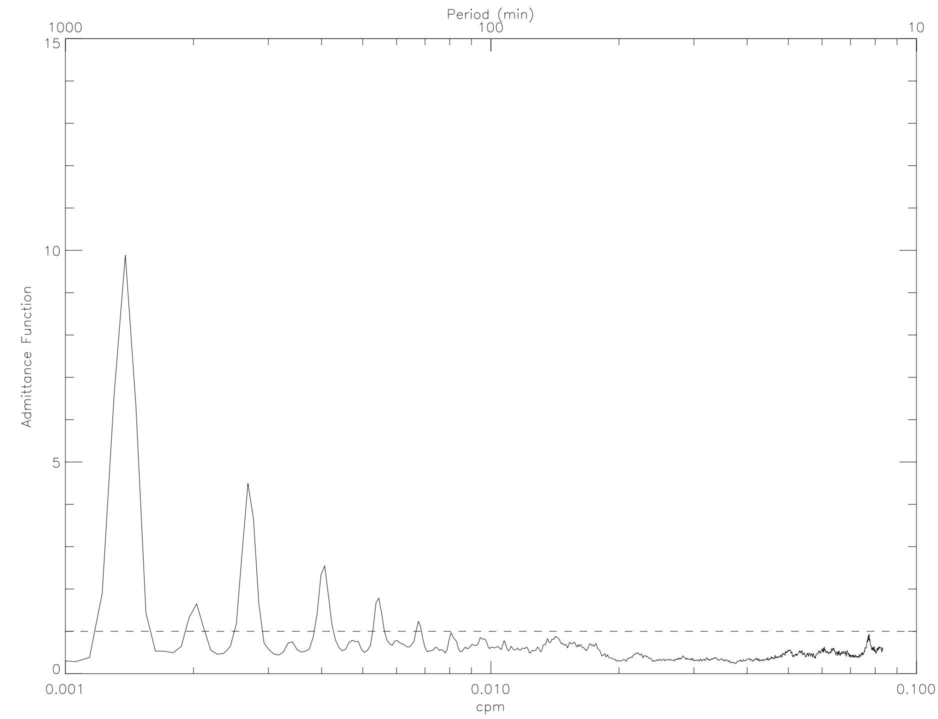

Figure 24: (a) **Power spectrum for the Solomon Islands, using data from 2002. The 95% confidence interval is indicated and the dashed line represents the hypothetical deep-water spectrum.** (b) **Topographic admittance function determined from the Solomon Islands power spectrum.**

a)

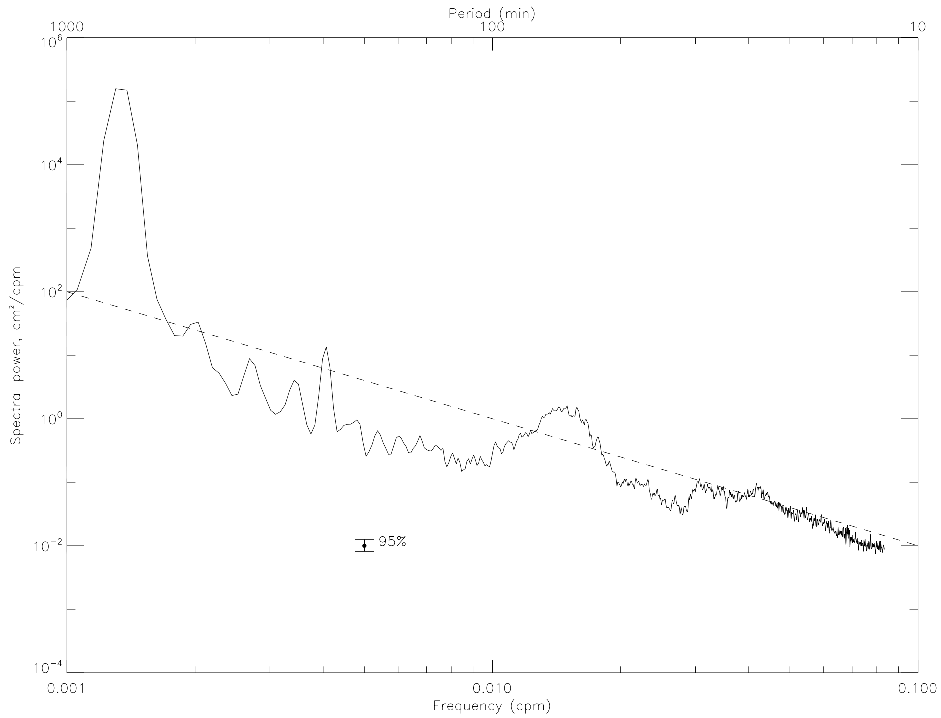

b)

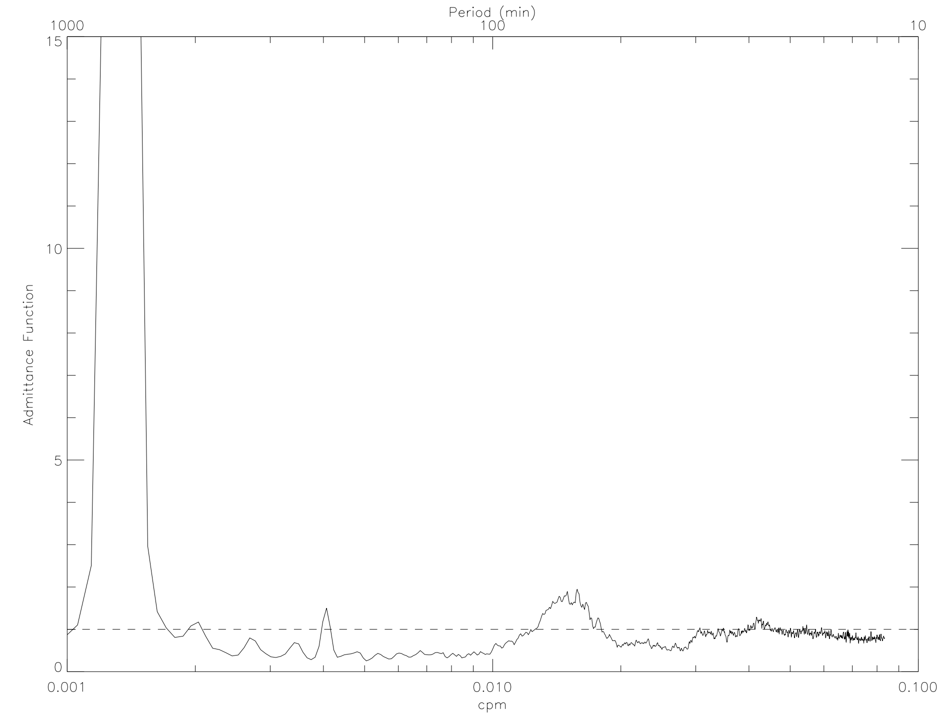

Figure 25: (a) **Power spectrum for Tonga, using data from 1 January to 1 December, 2002. The 95% confidence interval is indicated and the dashed line represents the hypothetical deep-water spectrum.** (b) **Topographic admittance function determined from the Tonga power spectrum.**

a)

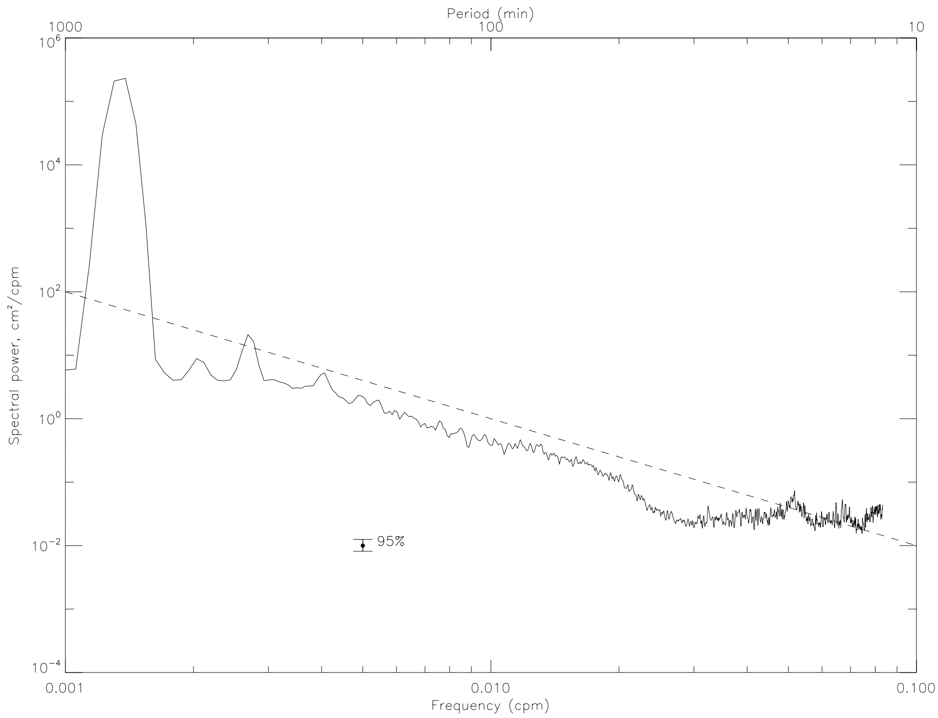

b)

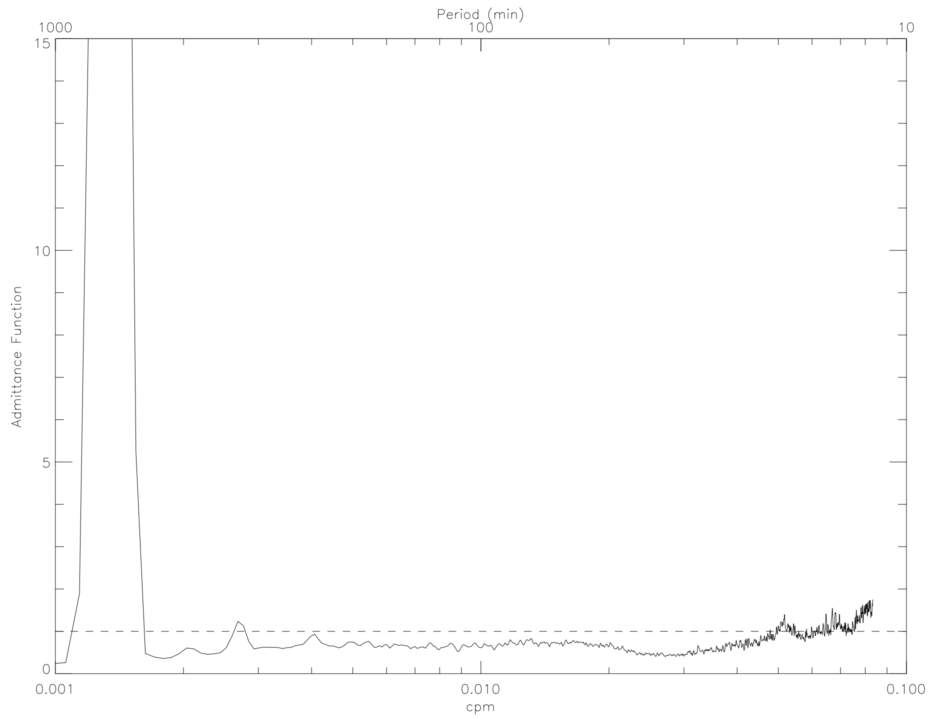

Figure 26: (a) **Power spectrum for Tuvalu, using data from 2002. The 95% confidence interval is indicated and the dashed line represents the hypothetical deep-water spectrum.** (b) **Topographic admittance function determined from the Tuvalu power spectrum.**

a)

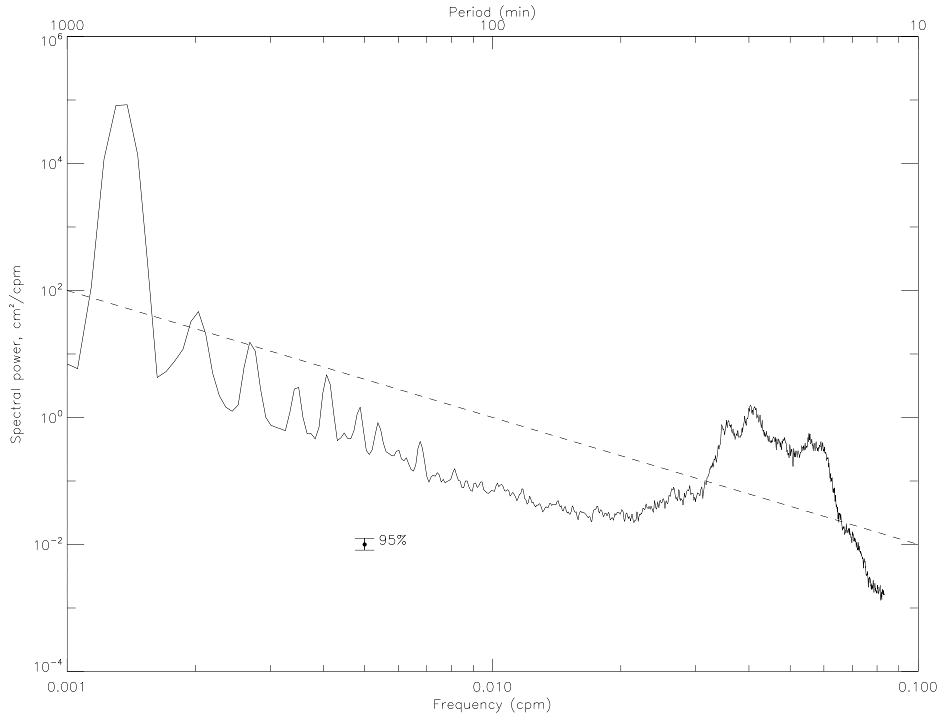

b)

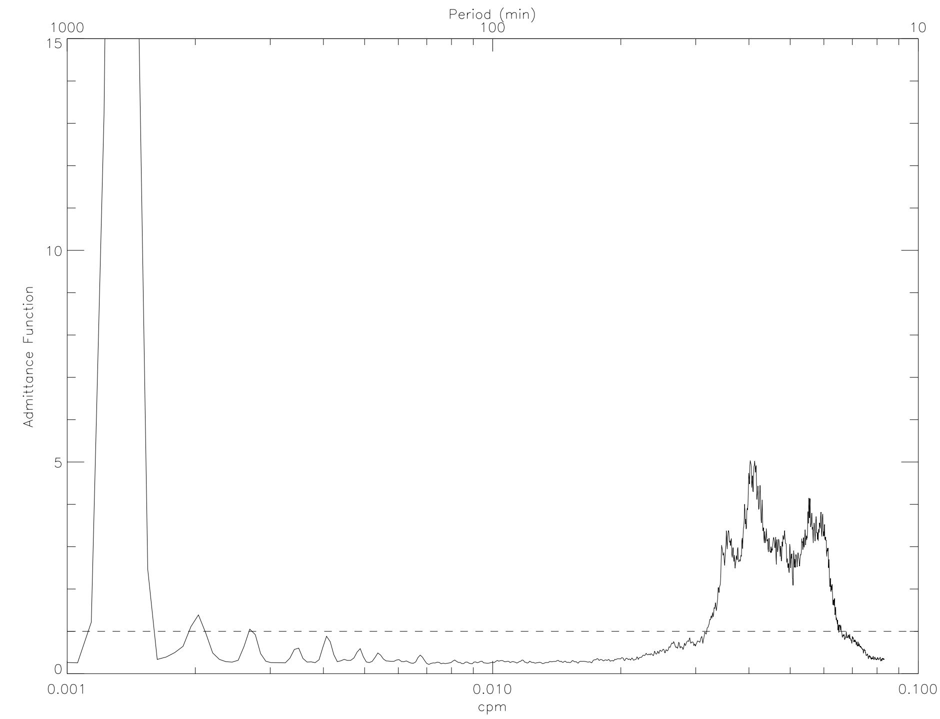

Figure 27: (a) **Power spectrum for Vanuatu, using data from 2002. The 95% confidence interval is indicated and the dashed line represents the hypothetical deep-water spectrum.** (b) **Topographic admittance function determined from the Vanuatu power spectrum.**

Location	Latitude	Longitude	Installation Date
Australian Baseline Array Gauges			
Broome	18°00'03.0"S	122°13'07.1"E	Nov 1991
Cape Ferguson	19°16'38.4"S	147°03'30.4"E	Sep 1991
Cocos Islands	12°07'0.1"S	96°53'30.9"E	Sep 1992
Esperance	33°52'15.2"S	121°53'43.3"E	Mar 1992
Hillarys	31°49'32.0"S	115°44'18.9"E	Nov 1991
Port Kembla	34°28'25.5"S	150°54'42.7"E	Jul 1991
Portland	38°20'36.4"S	141°36'47.4"E	Jul 1991
Rosslyn Bay	23°09'39.7"S	150°47'24.6"E	Jun 1992
Spring Bay	42°32'45.1"S	147°55'57.8"E	May 1991
Thevenard	32°08'56.2"S	133°38'28.8"E	Mar 1992
Pacific Array Gauges			
Raratonga, Cook Is	21°12'17.1"S	159°47'5.2"W	Feb 1993
Lautoka, Fiji	17°36'17.7"S	177°26'17.7"E	Oct 1992
Kiribati	1°21'54.2"N	172°55'58.8"E	Dec 1992
Marshall Is.	7°6'21.7"N	171°22'22.1"E	May 1993
Nauru	0°31'45.9"S	166°54'36.2"E	Jul 1993
Manus Island, PNG	2°2'31.5"S	147°22'25.6"E	Sep 1994
Samoa	13°49'36.4"S	171°45'40.7"W	Feb 1993
Solomon Is.	9°25'44.1"S	159°57'19.3"E	Jul 1994
Tonga	21°8'12.5"S	175°10'50.5"W	Jan 1993
Tuvalu	8°30'8.9"S	179°11'42.6"E	Mar 1993
Vanuatu	17°45'19.2"S	168°18'27.7"E	Jan 1993

Table 1: **List of tide gauges used in this study, their geographical coordinates and their date of installation.**

Site Name	Frequency Response			Continental Shelf width (km)
	Low Frequency	Mid Frequency	High Frequency	
Gauges located in a sheltered atoll lagoon				
Cocos Island	-1	0	+1	N/A
Kribati	+2	-1	-1	N/A
Marshall Islands	+1	+2	-1/+2	N/A
Gauges sheltered within an enclosed marina or harbour				
Tuvalu	-1	-1	+1	N/A
Port Kembla	-2	+3	+3	50
Hillarys	-2	+1	+3	80
Gauges located in an open bay in a relatively exposed location				
Nauru	+2	+2	+3	N/A
Samoa	-1	-2	+1	N/A
Spring Bay	-2	+3	+2	60
Thevenard	+2	+1	0	250
Rosslyn Bay	+1	+1	+2	300
Gauges located in an open bay but sheltered by reefs and/or islands				
Cape Ferguson	0	0	0	100
Tonga	-2	+1	+1	N/A
Gauges located in an open bay but sheltered by a headland or similar				
Raratonga	-2	-2	+2	N/A
Lautoka, Fiji	-2	+1	+1	N/A
Manus Island, PNG	0	+3	-1/+1	N/A
Solomon Islands	-1	-1	-2	N/A
Vanuatu	-2	-2	+3	N/A
Portland	-1	+3	+3	40
Esperance	-2	+2	+3	80
Broome	+1	-1	-1	500

Table 2: **The degree of attenuation or amplification for each site at low, middle and high frequency bands (see text), categorised by tide gauge site type.**

The Centre for Australian Weather and Climate Research is a partnership between CSIRO and the Bureau of Meteorology.